Gondwana Research xxx (2010) xxx–xxx

Contents lists available at ScienceDirect

Gondwana Research

journal homepage: www.elsevier.com/locate/gr

Late Archaean high-K granite geochronology of the northern metacratonic margin of the Archaean Congo craton, Southern Cameroon: Evidence for Pb-loss due to non-metamorphic causes

C.K. Shang [a,*], J.P. Liégeois [b], M. Satir [a], W. Frisch [c], E.N. Nsifa [d]

[a] Institut für Geowissenschaften, AB Mineralogie und Geodynamik, Eberhard-Karls-Universität, Wilhelmstrasse 56, D-72074 Tübingen, Germany
[b] Isotope Geology Section, Royal Museum for Central Africa, B-3080 Tervuren, Belgium
[c] Karl von Böhmerle Gasse 3, A-1140 Vienna, Austria
[d] Department of Earth Sciences, University of Yaounde I, BP 812 Yaoundé, Cameroon

ARTICLE INFO

Article history:
Received 27 September 2009
Received in revised form 31 January 2010
Accepted 11 February 2010
Available online xxxx

Keywords:
High-K granites
Pb–Pb evaporation
Zircon U–Pb
Pb-loss
metacratonization
Congo craton

ABSTRACT

High-K granitoids in the Archaean Congo craton are products of crustal differentiation by partial remelting of Archaean TTG, and in addition the remelting of charnockites at its northern metacratonic margin, the Ntem complex, in southern Cameroon. At the Sangmelima region of this metacratonized complex, high-K granites mostly occur as small intrusions and as pods, dykes and veins in TTG and charnockites. Zircon U–Pb analyses of these high-K granites show an important radiogenic Pb-loss, indicated by highly discordant U-rich fractions. Pb-loss in these smaller granitic intrusions appears to be due to continuous than discrete Pan-African diffusion and leaching, that characterizes larger charnockitic and tonalitic intrusions in the region, or a combination of both. The contributive effect of leaching due to later reactivations during the Phanerozoic cannot be ruled out. These multiple Pb-loss causes, and apparently disproportionate amounts of ^{206}Pb and ^{207}Pb loses, probably explain the irregular clustering of the highly discordant U–Pb data. However, an upper intercept age of 2751 ± 32 Ma and a lower intercept age of 300 ± 29 Ma are obtained. Most of the zircons, especially those from high-K granite veins, lost Pb from the entire grain with no domains remaining that reflect the original Pb isotopic composition. It was therefore impossible to obtain meaningful ^{207}Pb/^{206}Pb evaporation ages for such grains. Thus caution should be taken against use of the evaporation method for zircons that experienced severe Pb-loss. However, some whole zircons and zircon domains from larger granite bodies apparently retained their primary Pb isotopic composition and were dated successfully by the evaporation technique. They yielded reproducible ^{207}Pb/^{206}Pb ages between 2717 ± 9 Ma and 2724 ± 3 Ma, with a weighted mean of 2722 ± 2 Ma, interpreted as the minimum estimate of the crystallization age of the Sangmelima high-K granites. Similar Sr and Nd isotope signatures and Nd-model ages (3.04–3.25 Ga) as for the TTG and charnockite protoliths indicate that the high-K event did not add new juvenile material to the Archaean crust of the Congo craton but was the result of crustal differentiation.

1. Introduction

Magmatic rocks of the tonalite–trondhjemite–granodiorite (TTG) group and granodiorite–granite–monzogranite (GGM) group including high-K granites, and greenstone belts, (an association of metavolcanic sediments and mafic-ultramafic rocks), make up the bulk rock budget of Archaean cratons (e.g., Goodwin, 1991; de Wit, 1998; Condie and Benn, 2006; Cawood et al., 2009). Archaean cratons are also generally characterized by the occurrence of charnockites accreted at their margins (Celino and Botelho, 2005; Pouclet et al., 2007). Archaean crustal growth has been interpreted by the study of these rock formations (e.g., Luais and Hawkesworth, 1994; Moorbath and Kamber, 1998; Condie, 2000; Foley et al., 2002; Lobach-Zhuchenko et al., 2003, Sharma and Pandit, 2003; Shang et al., 2004a,b; Pouclet et al., 2007; Condie et al., 2009; Takam et al., 2009; Hegde and Chavadi, 2009). The high-K granites are generally younger and constitute the last major magmatic phase in Archaean terranes (de Wit, 1998; Tchameni et al., 2000; Kampunzu et al., 2003). They often outcrop in form of batholiths, but also as pods, veins and dykes. Studies on these rocks have proven to be a great contribution to the knowledge of crustal differentiation (e.g., Tepper et al., 1993; Borg and Clynne, 1998; Tchameni et al., 2000; Kampunzu et al., 2003; Shang et al., 2007). The challenge on the Archaean Congo craton is the scarcity of data to effectively set bench marks on rock succession and to substantiate crustal differentiation trends. This study is therefore

* Corresponding author. Tel.: +49 7071 29 73 160; fax: +49 7071 29 57 13.
E-mail addresses: cosmas@uni-tuebingen.de, shang004@yahoo.com (C.K. Shang), jean-paul.liegeois@africamuseum.be (J.P. Liégeois), satir@uni-tuebingen.de (M. Satir), frisch@uni-tuebingen.de (W. Frisch), nnsifa@yahoo.fr (E.N. Nsifa).

1342-937X/$ – see front matter © 2010 International Association for Gondwana Research. Published by Elsevier B.V. All rights reserved.
doi:10.1016/j.gr.2010.02.008

our contribution in data production on high-K granites of the Congo craton. It is aimed at dating the high-K granites of the Sangmelima region in the Ntem complex of the northern margin of the Congo craton in southern Cameroon, and to compare their age and geochemistry with known data in the region, for crustal differentiation assessment. But leaching of these rocks leads to serious consequences for geochronology including the analytical technique to employ. We will show that caution must be taken in dating zircons from such rocks by the evaporation technique. Furthermore, margins of Archaean cratons are highly affected by the activity of neighboring mobile belts. Here, we aim to demonstrate the case of the northern margin of the Archaean Congo craton in southern Cameroon, thrust over by the Central African fold belt. A comparison of high-K granite age data with geochronological data of TTG and charnockitic rocks will be made in order to establish a timetable for the Sangmelima granitoids and crustal differentiation stages at the northern margin of the Archaean Congo craton.

2. Geological background

The Congo craton is a large sub-circular mass of about 5 711 000 km^2 in area, and has a diameter of about 2500 km, comprising Archaean crust, early to mid Proterozoic fold belt and Proterozoic cover. Archaean formations form a ring of Archaean crusts of diverse sizes, (in clockwise succession from the south: Kasai–Angolan composite, Chaillu-Ntem complex, Gabon and Cameroon, Bouca, Bomu–Kibalian, Tanzania and Zambian), surrounding the unusually large, (1000–1200 km), sub-circular central late Proterozoic to Phanerozoic-filled Congo Basin (Goodwin, 1991). The Congo craton is almost entirely surrounded and partly indented by circumjacent Pan-African foreland belts: Mozambique belt on the east, Damara–Katanga–Zambezi belt on the south, West Congo–Kimezian belt on the west and the North Equatorial or Central African belt in the north. The northwestern margin of the Archaean Congo craton in Southern Cameroon is represented by the Ntem complex (Maurizot et al., 1986; Nédélec et al., 1990; Goodwin, 1991), which is bordered in the north by the Yaounde Group (e.g. Nzenti et al., 1988; Barbey et al., 1990; Mvondo et al., 2003; Toteu et al., 2006), of the Pan-African orogenic belt in Central Africa (Fig. 1). The two entities are delimitated by a major thrust fault of Pan-African age.

The Ntem complex comprises Palaeoarchaean to Mesoarchaean and Late Archaean charnockites, Mesoarchaean greenstone formations, Late Archaean TTG basement, dolerite dykes and high-K granites (Fig. 1). The sampled area in this present study, the Sangmelima region in the Ntem complex, constitutes the immediate margin area of the Congo craton with the Pan-African orogenic belt (Shang et al., 2004a,b). Here, high-K granites intrude TTG (e.g. Kornprobst et al., 1976; Nédélec, 1990; Shang, 2001; Shang et al., 2001, 2007). Late dolerite dykes in the area thought to be Eburnean in age (Toteu et al., 1994; Vicat et al., 1996), were recently identified as Late Archaean (Shang et al., 2007). This Late Archaean doleritic magmatism has been interpreted as the heat source for remelting TTG and charnockites and generating high-K granites (Shang et al., 2007), thus suggesting the coeval nature of doleritic magmatism and high-K granite genesis in the Ntem complex.

The Pan-African orogenic belt in Central Africa is actually part of the Neoproterozoic Oubanguides (Pin and Poidevin, 1987), extending from the Atlantic coastline in Cameroon to southwest Sudan, and is considered to mark the southern limit of the Saharan metacraton (Abdelsalam et al., 2002). This belt is one of the most important suturing orogens critical for Gondwanaland reconstruction. It is connected to the Sergipano belt to form the Pan-African–Braziliano mega-orogen considered to be due to the collision between the São Francisco–Congo craton, the West Africa craton and a Pan-African mobile domain (Castaing et al., 1994; Tetsopgang et al., 2008; Eriksson et al., 2009). The Yaounde Group of this mobile belt in southern Cameroon comprises two series, the Yaounde series and the Mbalmayo–Bengbis series, marked by deformed metasedimentary rocks and migmatites (Nzenti et al., 1988), that overthrust the Ntem complex and dips gently northwards. Rock types in the Yaounde series include chlorite-rich schists, garnet- and/or kyanite-bearing micaschists and garnet- and kyanite-bearing high-grade gneisses, thought to be derived from pelites and greywackes either in a continental margin or in a passive margin environment (Nzenti et al., 1988; Ngnotué et al., 2000). They are locally intruded by metamorphosed calc-alkaline dioritic plutons. Both the metasedimentary and the metadioritic rocks yielded a Neoproterozoic zircon U–Pb age of 620 ± 10 Ma (Penaye et al., 1993; Toteu et al., 1994, 2006).

Two important reactivation episodes affected the Ntem complex in Eburnean and Pan-African times. Old Rb–Sr whole-rock data from Lasserre and Soba (1976), though seemingly unreliable, suggest recrystallization between 2400 and 1800 Ma. Shang et al. (2004a) reported Rb–Sr biotite ages between 2299 and 2064 Ma, (confirming Lasserre and Soba 1976 data), and interpreted them as Eburnean reactivation fingerprints in the Sangmelima region of the Ntem complex. Toteu et al. (1994) reported similar peak U–Pb zircon metamorphic ages from the Nyong series of ca. 2050 Ma, and Lerouge et al. (2006) re-interpreted these ages as syntectonic plutonism ages. These ages mark the Eburnean orogeny in the area. Retrograde metamorphism, characterized by mineral transformations (pyroxene → amphibole, biotite → chlorite, feldspars → sericite and/or damourite) in TTGs of the Ntem complex near the thrust border to the Pan-African mobile belt, as well as Pan-African U–Pb lower intercept ages in these rocks (e.g. Toteu et al., 1994; Shang et al., 2004b; Takam et al., 2009), and in supracrustal formations from the southeastern Archaean Congo craton in Uganda (e.g. Appel et al., 2005), indicate that the Pan-African orogeny has more pronounced imprints on the Congo craton than hitherto thought. In the following lines, we will describe the petrographic and geochemical characteristics of Sangmelima high-K granites and show, using U–Pb data, the combined imprints of Pan-African and recent reactivation effects in these rocks.

3. Petrography

The Sangmelima high-K granites constitute a suite of rocks that include monzogranite and syenogranite. They occur as leucocratic pods and tongues in association with mafic restite, as well as small-scale pegmatitic and aplitic veins and dykes in TTGs and charnockites. The restite is dominated by amphibole and biotite. Locally, meter to tens of meter scale high-K granite dykes intrude TTG and charnockites. Primary mineral assemblage includes phenocrystic and perthitic microcline (Fig. 2a), albitic plagioclase and quartz as major phases. Myrmekites commonly occur at the contact between microcline and plagioclase (Fig. 2b). Mafic minerals include reddish-brown biotite, minor clinopyroxene and hornblende. Zircon, apatite and opaque oxides constitute the accessory phases.

4. Analytical techniques

4.1. Major and trace element geochemistry

Major and trace element analyses were performed on fused glass beads of whole-rock powders at the University of Tübingen using a Bruker AXS S4 Pioneer spectrometer, while REE elements were

Fig. 1. Regional geological map of the north-western margin of the Archaean Congo craton (Ntem complex), and thrust contact with the Pan-African fold belt in Southern Cameroon, modified after Maurizot et al. (1986). Simplified geological map of the Sangmelima region showing high-K granite distribution and localization of the analyzed samples.

Please cite this article as: Shang, C.K., et al., Late Archaean high-K granite geochronology of the northern metacratonic margin of the Archaean Congo craton, Southern Cameroon: Evidence..., Gondwana Research (2010), doi:10.1016/j.gr.2010.02.008

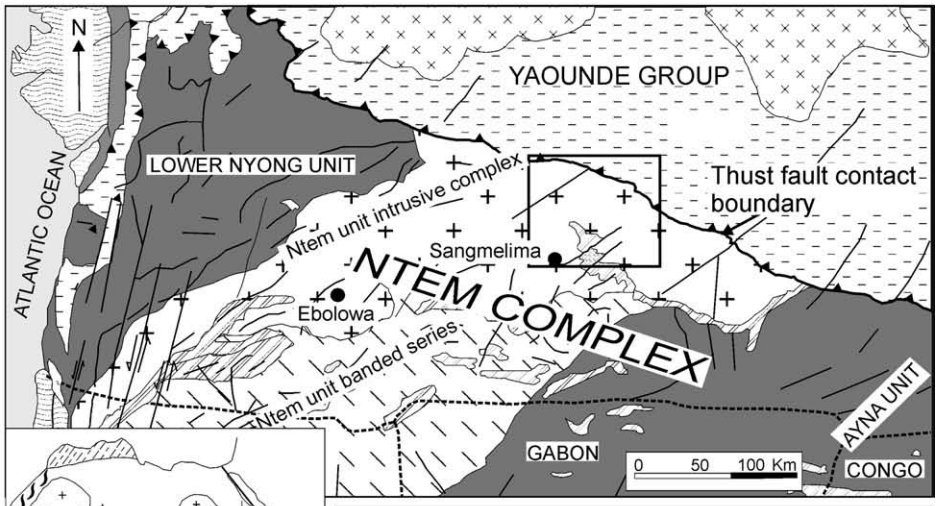

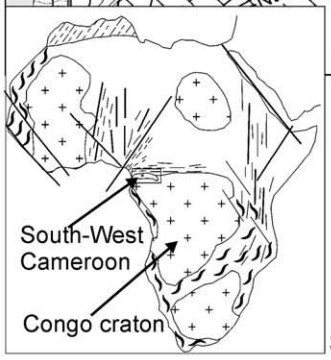

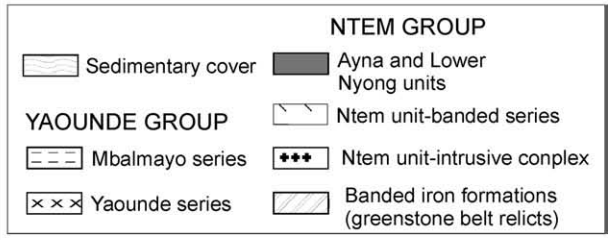

South-West Cameroon (after Maurizot et al., 1986)

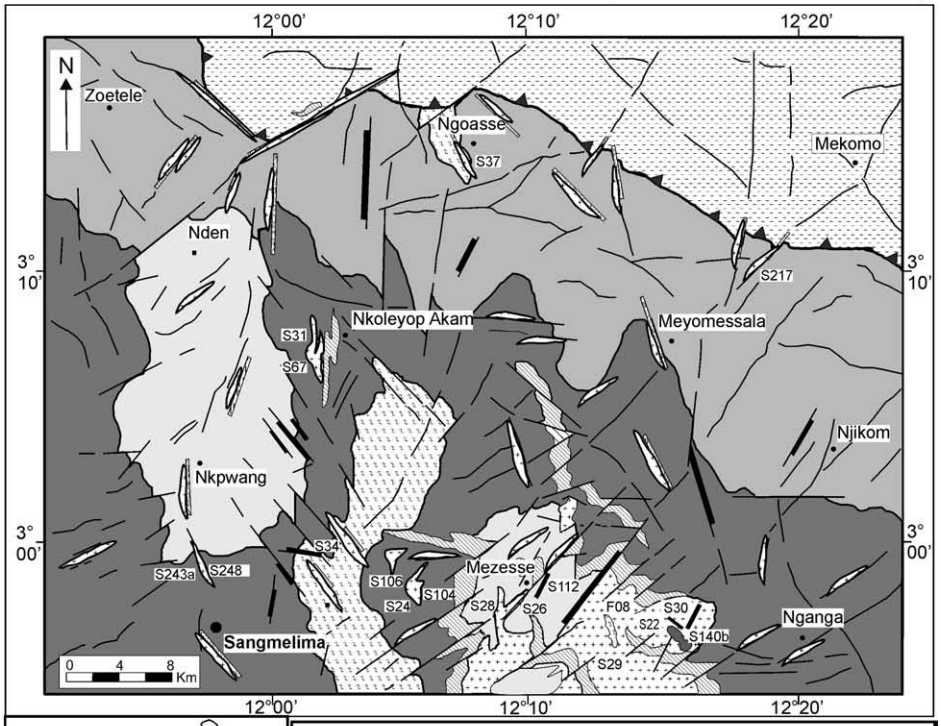

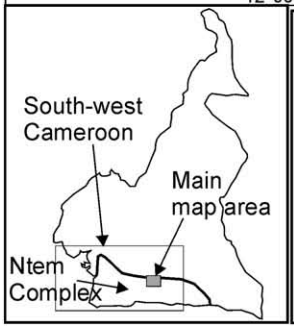

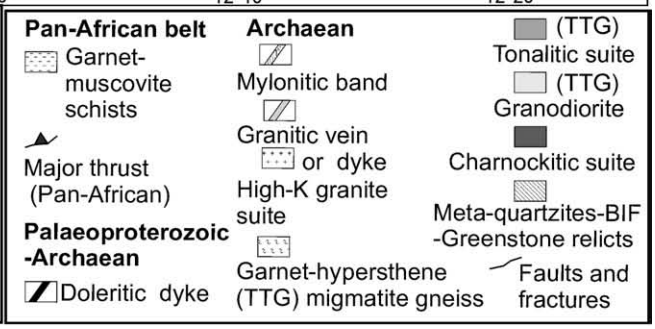

Please cite this article as: Shang, C.K., et al., Late Archaean high-K granite geochronology of the northern metacratonic margin of the Archaean Congo craton, Southern Cameroon: Evidence..., Gondwana Research (2010), doi:10.1016/j.gr.2010.02.008

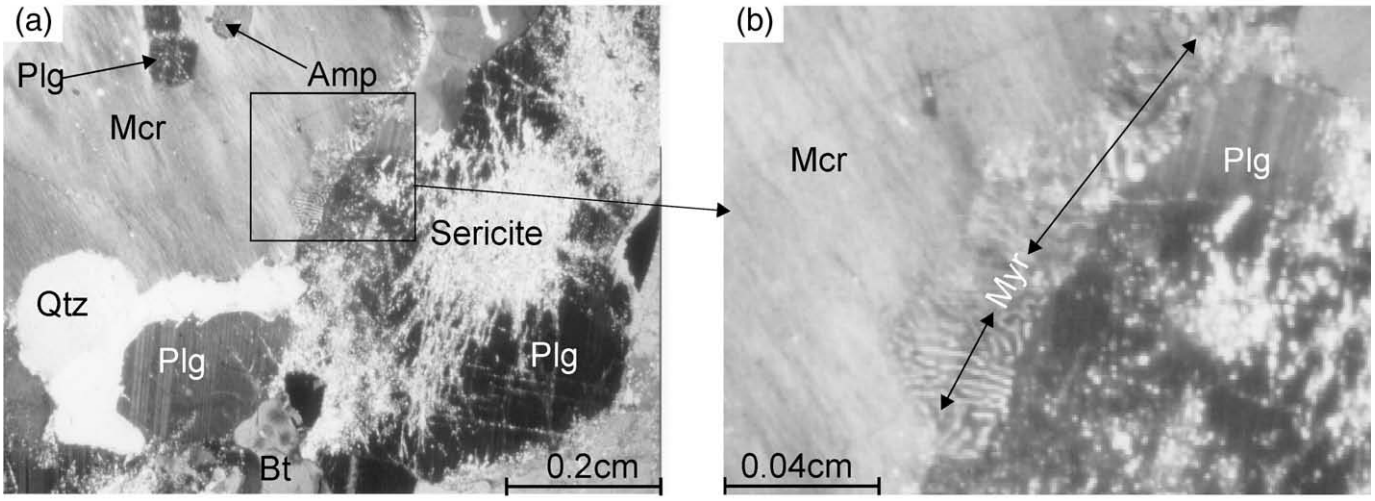

Fig. 2. Thin section view: (a) showing pegmatitic texture (Mcr — microcline, Plg — plagioclase, Qtz — quartz, Bt — biotite, Amp — amphibole), and perthitic microcline containing plagioclase and amphibole inclusions, (b) myrmekitic intergrowth between microcline and plagioclase.

measured by ICP-MS at the laboratory of RMCA in Tervuren, Belgium. Loss on ignition, (LOI), was determined after igniting 1 g of rock sample powder in quartz crucibles at 1050 °C for 1 h. Relative analytical uncertainties are estimated to be less than 1% for major elements and between 2% and 5% for trace elements.

4.2. Rb–Sr and Sm–Nd isotopes

Sr and Nd isotopes were separated from dissolved whole-rock powders by standard chromatographic techniques. Analyses were performed using a Finnigan MAT 262 multi-collector thermal ionisation mass spectrometer (TIMS), in static collection mode, at the University of Tübingen. Sr was loaded with a Ta-Hf activator and measured on a single W filament. Rb was loaded as a chloride and Sm and Nd were loaded as phosphates and measured in a double re-filament configuration mode. The $^{87}Sr/^{86}Sr$ ratios were normalized to $^{86}Sr/^{88}Sr = 0.1194$, the $^{143}Nd/^{144}Nd$ ratios to $^{146}Nd/^{144}Nd = 0.7219$, and Sm isotopic ratios to $^{147}Sm/^{152}Sm = 0.56081$. Analyses of 24 separate loads of Ames metal gave a $^{143}Nd/^{144}Nd$ ratio of 0.512125 ± 10. NBS 987 Sr standard yielded $^{87}Sr/^{86}Sr$ ratio of 0.710259 ± 12 ($n = 28$). Total procedural blanks (chemistry and loading) were <200 pg for Sr and <100 pg for Nd. Least-square regression of the Rb–Sr and Sm–Nd isotopic data, with assessment of fit using the mean square of the weighted deviates (MSWD), were calculated after Ludwig (2003). All errors are quoted at the 2σ level. Nd-model ages and ε_{Nd} values were calculated using present day CHUR values of 0.1967 for $^{147}Sm/^{144}Nd$ (Jacobson and Wasserburg, 1980) and 0.512638 for $^{143}Nd/^{144}Nd$ (Goldstein et al., 1984). Model ages were also determined using depleted mantle values as given in Nelson and DePaolo (1988). Decay constant for ^{87}Rb (1.42×10^{-11} a^{-1}) was taken from Steiger and Jäger (1977) and for ^{147}Sm (6.54×10^{-12} a^{-1}) from Lugmair and Marti (1978).

4.3. Zircon cathodoluminescence and Pb–Pb and U–Pb geochronology

All analyses were done at the University of Tübingen. Zircon grains were separated from 200 to 125 μm and 125 to 63 μm sieved rock fractions by standard separation techniques (milling, Wilfley Table, magnetic and heavy liquid separation). The zircon grains were studied for morphological characterization using binocular and transmitted light microscopes to determine their typologic distribution (e.g., Pupin, 1980). Zircon internal structure was studied by cathodoluminescence (CL), using the electron microprobe JEOL Superprobe, JXA-8900RL, working with accelerating potential of 15 kV and 15–10 nA current beam.

The technique used for zircon evaporation is that developed by Kober (1986, 1987). $^{207}Pb/^{206}Pb$ ages were obtained from chemically untreated zircons. Pb isotopes were measured in the mass sequence 206–207–208–204–206–207 with the Finnigan MAT 262 TIMS. Preheating at temperatures of ca. 1350–1370 °C served as zircon cleaning procedure. Temperatures of the evaporation filament were increased in 20 °C steps during repeated evaporation. All data were corrected for common Pb according to Cocherie et al. (1992). The common Pb corrected $^{207}Pb/^{206}Pb$ ratios normally define a Gaussian distribution and the mean of the $^{207}Pb/^{206}Pb$ ratios was derived from this distribution. $^{207}Pb/^{206}Pb$ ratio errors are two sigma values and refer to the last digits. Our technique has been tested for reproducibility on natural zircons from the Phalaborwa igneous complex, South Africa (Eriksson, 1984; Verwoerd, 1986) and zircon 91,500 from the Kuehl Lake, Ontario, Canada (Wiedenbeck et al., 1995), the results of which are published in Chen et al. (2002). During the course of this study, we also tested a new standard (e.g. Sláma et al., 2008, Table 1).

For U–Pb isotope dilution analyses, zircons were washed in 6 N HCl and 7 N HNO_3 for half an hour at room temperature, and rinsed with ultra clean H_2O. A mixed ^{205}Pb–^{235}U spike was added to the sample before dissolution using HF at 200 °C for 6 days in Parr bomb (e.g. Parrish, 1987). Separation and purification of U and Pb was done in minicolumns with a 40-μl bed of AG1-X8 (100–200 mesh) anion exchange resin in a HBr and HCl medium. U and Pb were loaded on outgassed Re filaments with 0.1 N Si gel and H_3PO_4 and run on MAT 262 TIMS. Pb isotopes were measured at about 1200 °C in static collection mode with ^{204}Pb measured on a secondary electron multiplier (SEM) in ion-counting mode. U was analyzed between 1300 °C and 1350 °C by ion counting. Procedure blanks ranged between 5 and

Table 1
Pb evaporation data for standard material Plešovic zircon, Sláma et al. (2008).

Grain	Number of ratios	Evaporation temperature	Mean of $^{207}Pb/^{206}Pb$ ratios	$^{207}Pb/^{206}Pb$ age (Ma)
1	149	1400 °C	0.053137 ± 56	334.7 ± 3.3
2	150	1400 °C	0.053224 ± 47	337.4 ± 4.1
3	49	1400 °C	0.053196 ± 74	336.4 ± 3.2
Mean age		MSWD = 0.57	95% confidence	336 ± 2
Reference age (ID TIMS)				337.13 ± 0.37

Please cite this article as: Shang, C.K., et al., Late Archaean high-K granite geochronology of the northern metacratonic margin of the Archaean Congo craton, Southern Cameroon: Evidence..., Gondwana Research (2010), doi:10.1016/j.gr.2010.02.008

Table 2
Major and trace element concentrations (in wt.% and ppm respectively) for Sangmelima high-K granitoids.

Sample	S243a	S24	S104	S34	S30	S29	S37	S22	S140b	S28	S112	S217	S26	S106a	S31	S67	F08
SiO_2	66.3	66.7	67.9	68.3	70.8	72.5	72.7	73.0	73.1	73.2	73.4	73.7	73.8	74.4	74.9	75.0	76.8
TiO_2	0.29	0.28	0.22	0.19	0.25	0.29	0.14	0.15	0.07	0.20	0.25	0.20	0.24	0.08	0.09	0.04	0.04
Al_2O_3	16.9	16.2	16.4	14.9	13.8	13.8	14.9	14.3	14.54	14.4	14.4	14.1	13.3	14.4	14.0	13.1	13.7
Fe_2O_3	2.61	2.86	2.99	3.47	3.02	2.30	1.62	1.14	1.48	1.59	1.69	2.05	1.76	1.06	0.60	0.25	0.40
MnO	0.03	0.02	0.03	0.05	0.03	0.02	0.06	0.02	0.01	0.03	0.03	0.02	0.02	0.02	0.01	0.01	0.01
MgO	0.96	0.60	0.56	2.74	0.09	0.41	0.82	0.26	0.01	0.47	0.66	0.36	0.50	0.54	0.15	0.01	0.12
CaO	2.27	2.00	2.19	1.59	0.79	1.57	1.89	0.75	0.90	1.91	1.47	1.69	0.89	2.00	1.52	0.37	1.47
Na_2O	3.52	3.01	3.32	3.02	3.36	3.08	3.36	3.19	3.42	3.67	3.10	3.05	2.63	3.20	3.39	1.95	3.46
K_2O	5.36	6.70	5.33	5.02	6.38	4.58	4.05	6.59	5.48	3.98	4.63	3.77	6.16	4.36	4.49	7.86	4.41
P_2O_5	0.14	0.26	0.18	0.05	0.04	0.07	0.04	0.13	0.07	0.06	0.04	0.05	0.05	0.03	0.05	0.01	0.02
LOI	0.78	0.79	0.46	0.31	0.46	0.73	0.51	0.35	0.42	0.37	0.32	0.66	0.33	0.58	0.32	0.29	0.37
Total	99.06	99.48	99.60	99.61	98.97	99.35	100.02	99.82	99.51	99.83	99.94	99.69	99.67	101.03	99.42	98.93	101.10
$Na_2O + K_2O$	8.88	9.71	8.65	8.04	9.74	7.66	7.41	9.78	8.90	7.65	7.73	6.82	8.79	7.56	7.88	9.81	7.87
Na_2O/K_2O	0.68	0.45	0.62	0.60	0.50	0.67	0.83	0.48	0.63	0.93	0.67	0.81	0.43	0.74	0.76	0.25	0.69
Ab/An	2.9	2.6	2.9	3.1	7.8	3.4	2.9	8.5	7.2	3.2	3.7	3.2	4.9	2.5	3.6	5.6	3.7
A/CNK	1.07	1.03	1.08	1.12	1.00	1.07	1.12	1.04	1.13	1.04	1.10	1.16	1.06	1.06	1.06	1.06	1.05
Mg#	42.0	29.4	27.1	61.0	05.6	26.3	50.0	30.9	01.1	37.0	43.42	25.80	36.1	50.2	33.1	06.7	38.0
Ba		6052		2637	126	1359	2032	866		1514			1427	2790	2059	3919	2459
K	44,488	55,610	44,239	41,666	52,954	38,014	33,615	54,697	45,484	33,034	38,429	31,291	51,128	36,188	37,267	65,238	36,603
Nb		2		3	4	3	4	2		3			29	0	6	1	0
Ni		8		23	3	9	10	3		10			0	0	5	6	0
Rb		128		90	555	129	68	322		152			246	83	118	186	98
Sr		414		235	57	169	189	196		312			224	584	297	412	286
V		50		28	5	24	9	7		20			19	24	5	12	9
Y		13		4	26	14	16	24		13			27	3	11	9	3
Zn		27		57	25	29	16	19		30			39	1	12	2	0
Zr		179		126	22	217	118	23		153			120	144	135	36	116
La		122.8		–	28.0	80.5	–	26.9		16.4			44.9	29.8	11.8	7.9	8.6
Ce		198.1		–	47.3	137.5	–	47.7		–			86.1	–	18.75	11.71	–
Pr		18.3		–	–	13.3	–	–		–			8.8	–	1.60	0.84	–
Nd		57.5		13.8	54.3	42.0	21.2	20.9		8.2			27.3	–	4.99	2.44	–
Sm		5.81		2.6	3.3	5.7	–	4.0		–			5.0	–	0.52	0.43	–
Eu		0.9		0.7	0.7	0.8	0.4	0.4		–			0.34	1.2	0.38	0.62	0.5
Gd		3.91		–	–	3.9	–	–		–			3.70	–	0.66	0.18	–
Dy		1.21		–	–	1.66	–	–		–			3.42	–	0.39	0.09	–
Ho		0.17		–	–	0.21	–	–		–			0.66	–	0.05	0.05	–
Er		0.40		–	–	0.49	–	–		–			2.02	–	0.25	0.05	–
Yb		0.3		0.5	0.7	0.3	1.6	1.1		1.2			2.49	–	0.23	0.10	–
Lu		0.03		–	–	0.04	–	–		–			0.40	–	0.03	0.01	–
Hf		3.4		–	–	5.8	–	–		–			4.18	–	3.91	0.70	–
Ta		0.05		–	–	0.05	–	–		–			8.55	–	0.45	0.05	–
W		0.50		–	–	0.81	–	–		–			1.07	–	0.70	0.41	–
Pb		42.7		20.9	16.4	30.7	14.10	24.2		33.3			33.3	10.8	16.9	23.5	9.0
Th		81.6		–	26.9	55.6	–	30.3		16.7			40.0	7.2	10.8	5.04	6.8
U		0.86		3.4	3.4	2.06	–	1.2		4.8			22.2	6.7	2.5	1.5	4.5
ΣREE		538.4		41.9	181	382	37.7	156.7		80.6			294.6	55.7	74.8	55.6	29.4
K/Rb		434.5		463	95.4	294.7	494.3	169.9		217.3			208	436	316	351	374
Rb/Sr		0.309		0.38	9.74	0.76	0.36	1.64		0.49			1.10	0.14	0.40	0.45	0.34
Th/U		94.9		–	7.9	27.0	–	25.3		3.5			1.8	1.1	4.4	3.3	1.5
La_N/Yb_N		285.3		–	21.0	180.9	0.17	16.5		9.4			12.18	–	34.6	52.9	–
Eu/Eu*		0.57		–	–	0.52	–	–		–			0.24	–	1.96	6.91	–

10 pg for both U and Pb. Fractionation factors for U and Pb correspond to 0.1% per atomic mass unit. Corrections for remaining initial common Pb after the correction for tracer and blank were done following the model of Stacey and Kramers (1975). The U–Pb data were evaluated and plotted using Isoplot version 3.0 from Ludwig (2003).

5. Results

5.1. Major and trace element geochemistry

Whole-rock silica content (66–77% SiO_2; Table 2) marks the felsic composition of the rocks. The rocks are peraluminous (A/CNK = 1.00–1.16, Fig. 3a) and also marked by high alkali contents ($Na_2O + K_2O$ = 6.8–9.8) and low Na_2O/K_2O ratios (0.25–0.93) (Fig. 3b). Their K_2O contents are typical of high-K and shoshonitic rocks (Fig. 3c). In the sliding normalization diagram (Fig. 3d) where each rock is normalized to a virtual rock from the reference series (NYTS-normalization to the Yenchichi–Telabit series) that has the same silica content (Liégeois et al., 1998), the analyzed samples plot in the potassic differentiation field. This character is confirmed in the Na_2O–K_2O–Ca0 diagram (Fig. 3e). In the normative Q–A–P diagram (Fig. 3f) the analyzed samples plot in the monzogranite and syenogranite fields. In the SiO_2 versus the $FeO_t/(FeO_t + MgO)$ diagram (Fig. 3 g), the samples range from the magnesian to the ferroan field, and in the SiO_2 versus $Na_2O + K_2O$–CaO diagram, they range form the calcic to the alkalic fields (Fig. 3h), similar to peraluminous leucogranites (Frost et al., 2001).

The rocks are enriched in LILE and depleted in HFSE (Table 2). Characteristic subduction related features (e.g. negative Nb and Ti anomalies, Fig. 4a, and negative Ta anomalies, not shown) are inherited from their TTG and charnockitic protoliths (Shang et al., 2007). They are enriched in LREE. Total REE abundances range from 36 to 236 ppm. La_N/Yb_N ratios distinguish two groups of samples; one group of five samples (three shown, Fig. 4a, and two others in Table 2 not shown because of the incomplete data set), with low ratios (0.17 to 21), and another group of two samples (S24, S29) with high ratios (181 and 285) and steeper REE patterns (Fig. 4b). Samples with overall low REE abundances show strong positive Eu anomalies ($Eu/Eu^* = 1.96$ and 6.91), probably explained by high plagioclase or potassic feldspar content, while samples with high REE concentrations display more negative Eu anomalies (Fig. 4b). Sample S67 with lowest total REE abundance and low Zr abundance (Table 2) shows strong depletion in HREE with near typical Archaean TTG pattern, a probably inherited feature from the TTG protolith (e.g. Shang et al., 2007). Whatever the case, the pattern is characteristic of REES composition of melt extraction during zircon crystallization. Alternatively, it could mark a melt from a garnet-rich source. Sample S26 shows enriched HREE pattern (Fig. 4b), probably indicating the presence of zircon that concentrate HREEs or may be a signature of garnet-free source.

5.2. Zircon morphology and internal structure

Zircon typologic distribution (Pupin, 1980) as based on zircon grain morphology is presented in Table 3. It is worth recalling here that Pupins (1980) zircon typology is a classification of zircon populations based on the analyses of zircon crystal pyramidal and prismatic face intersections with crystallographic axes leading to various zircon population types, named following letters of the alphabet (A, B, P, S, etc). The abundance of zircon crystals in some population types leads to divisions into subtypes (1 to 25). The main types show 0, 1 or 2 prisms, i.e. {100}, {110} in combination with either one of the three pyramids {101}, {211} or {301}, or the arrangement {101}+{211} (Pupin, 1980).

Zircons crystals in this study range from ~65 to ~120 μm in thickness and up to 180 μm along the longest crystal axis. They are euto sub-anhedral, long and needle-like, or small and short and infrequently thick. A couple of twin crystals were observed. The zircon crystals are light brown to yellow, transparent and occasionally translucent, and sometimes contain inclusions. They fall into P, S, AB and D types (Table 3). Most belong to P_2, P_3 and S_{10}, S_{15} subtypes, each subtype making about 10–20% of the total crystal counts. I.T and I.A typologic indices, (I.T being the vertical indice of prism faces and I.A, the horizontal indice of pyramidal faces, Pupin, 1980), indicate moderate to high values. P_2 and P_3 subtypes and S_{10} and S_{15} subtypes are marked by the same I.T values of 400–500 but different I.A values of 700 and 600 respectively. P_4 and P_5 subtypes have I.T values of 600–700 and the same I.A value of 700 with the D subtype which is marked by an I.T value of 800. $AB_{1,2,3}$ subtypes have the lowest I.T value of 100 and the I.A value range of 200–400. S_1, S_7 and S_{12} subtypes define I.A values of 200–300 and I.T values of 300–500 while S_{25} is characterized by I.T and I.A values of 700 and 600, respectively. The majority of the analyzed zircon crystals define monzogranite zircon types in agreement with the whole-rock geochemical classification (Fig. 3f) and Pupin's (1980; Fig. 3) classification. They fall in or close to stock 4 (Pupin, 1980; Fig. 7), that marks calc-alkaline series granite field, stocks 5, 6 and 7 that mark subalkaline, alkaline and tholeiitic series granite fields respectively.

A preliminary correlation test of zircon type, fractures and U content in this study showed that P-type zircons have few cracks, low U content and lower degrees of discordance, suggesting low amounts of Pb-loss. On the other hand, S-type zircons with short prism faces contain many cracks, have high U content, are more metamict and show high degrees of discordance, suggesting high amounts of Pb-loss. As a result, more P-type zircons, when possible, were preferably selected for U–Pb and Pb–Pb analyses than S-type zircons.

Representative polished CL sections of zircons (Fig. 5) show internal structures that suggest a complex geologic history. A number of crystals (e.g. S24-1, S24-4, S31-4, S31-6, S31-8, S112-11, S112-13) show microstructural homogeneity with magmatic oscillatory zoning of CL dark and bright bands that characterize variable trace element and REE concentrations (e.g., Köppel and Sommerauer, 1974; Hanchar and Miller, 1993, Hanchar and Rudnick, 1995; Kempe et al. 2000; Corfu et al., 2003; Nasdala et al. 2003). Needle-shaped crystals tend to show less CL bright zones, a feature attributed to crystallinity (e.g. Nasdala et al., 2002) or lattice defects (Pidgeon, 1992; Geisler and Pidgeon, 2001). Some grains show unzoned or faintly zoned patches (S24-7) and discontinuous CL bright bands (e.g. S31-6, S29-1, S29-3, S248-3), representing melt resorption–dissolution features and recrystallized portions, that are often accompanied by Pb and U loss (e.g., van Breemen et al., 1987; Vavra, 1990; Pidgeon, 1992). Backscattered images (S112-3Bs, S112-12BS) and some CL images (S31-4, S31-7, S29-9, S112-4) show radial fractures and channels, evidence that the primary magmatic zircon has been affected by brittle deformation. Occurrence of a meshwork of metamict zircon due to radiation damage (S31-1 and S248-4), suggests high U content. This feature, in addition to fractures, favours Pb-loss by diffusion and leaching. CL images show no inherited cores.

Fig. 3. Geochemical characterization of Sangmelima high-K granitoids: (a) showing peraluminous composition in the $Al_2O_3/(CaO + Na_2O + K_2O)$ versus $Al_2O_3/(Na_2O + K_2O)$ diagram; (b) Na_2O/K_2O versus SiO_2 showing low Na_2O/K_2O ratios (<1) and plots in the K-granite field; (c) K_2O versus SiO_2 diagram portraying high-K and shoshonitic composition; (d) Mean[Zr–Ce–Sm–Y–Yb]NYTS versus mean[Rb–U–Th–Ta]NYTS sliding normalization plot showing potassic affinity of the analyzed samples (NYTS = normalization to the Yenchichi–Telabit series, Liégeois et al., 1998); e) Na–K–Ca diagram confirming a potassic calc-alakline affinity of the high-K granite suite members; (f) Q–A–P triangular diagram with sample plots in the monzogranite and syenogranite fields; (g) SiO_2 versus $FeO_t/(FeO_t + MgO)$ diagram showing both magnesian and ferroan compositions; (h) SiO_2 versus $Na_2O + K_2O$–CaO diagram; samples range from the calcic to alkalic fields.

Please cite this article as: Shang, C.K., et al., Late Archaean high-K granite geochronology of the northern metacratonic margin of the Archaean Congo craton, Southern Cameroon: Evidence..., Gondwana Research (2010), doi:10.1016/j.gr.2010.02.008

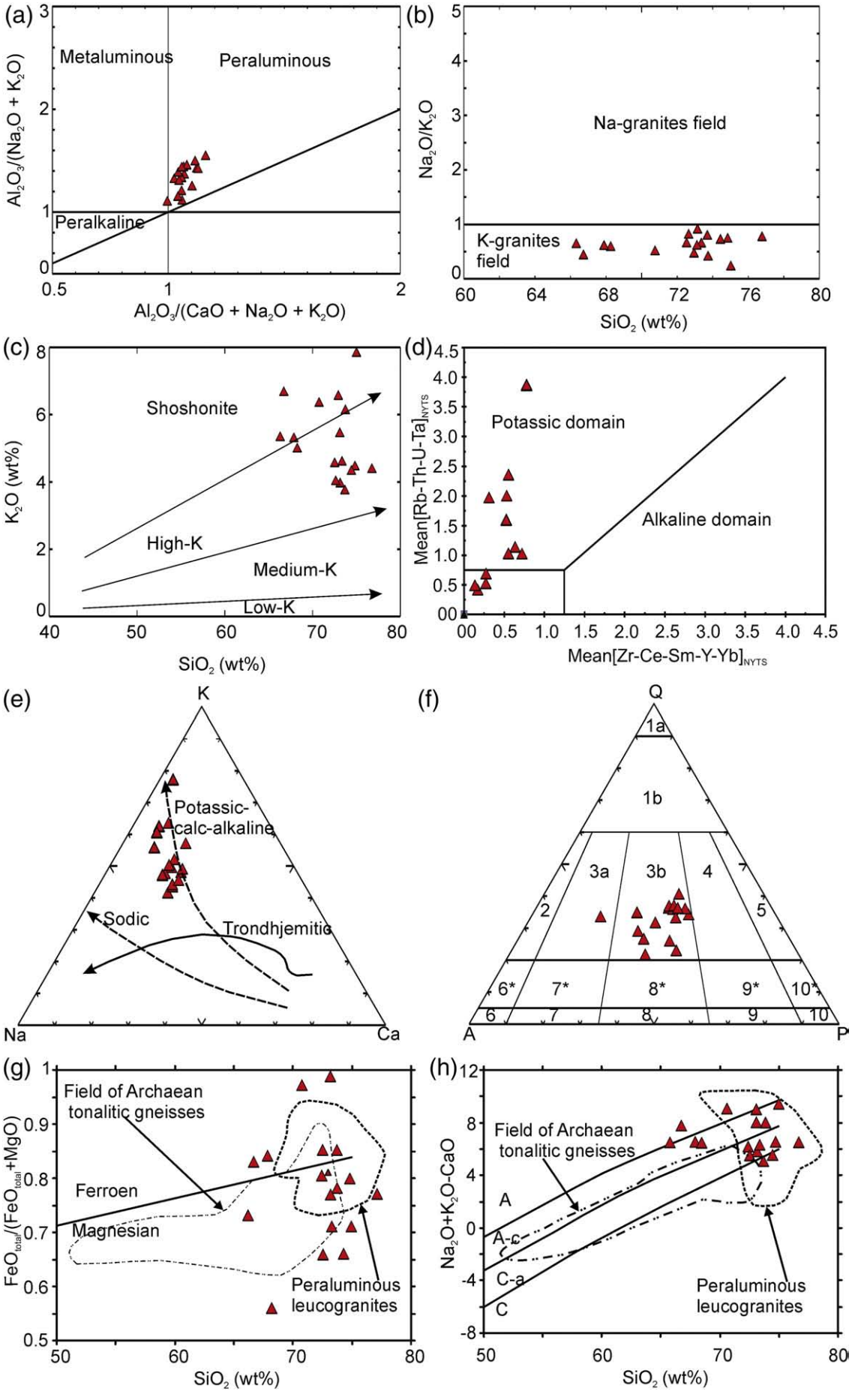

Please cite this article as: Shang, C.K., et al., Late Archaean high-K granite geochronology of the northern metacratonic margin of the Archaean Congo craton, Southern Cameroon: Evidence..., Gondwana Research (2010), doi:10.1016/j.gr.2010.02.008

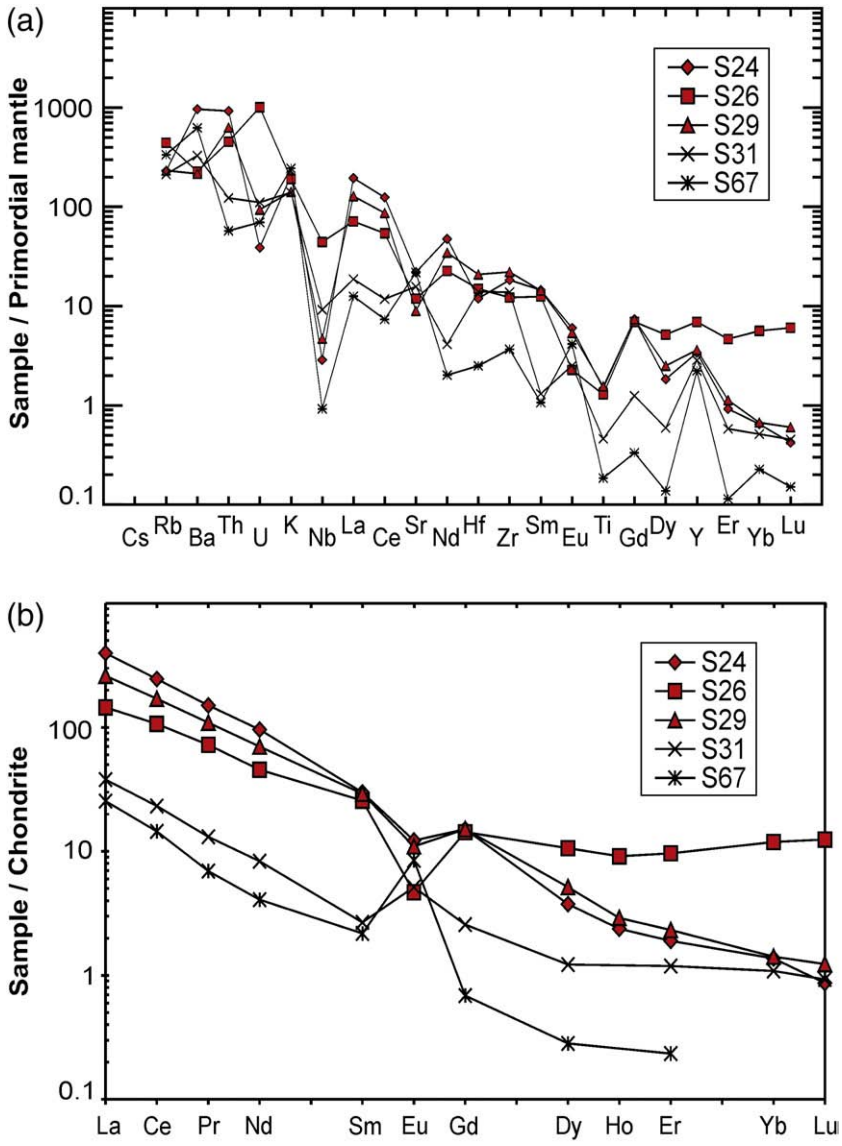

Fig. 4. (a) Primodial mantle normalized spidergrams showing negative Nb and Ti characteristic subduction anomalies, interpreted as inherited features from the TTG protolith; (b) chondrite normalized REE patterns showing two samples marked by positive Eu anomalies and three others marked by negative Eu anomalies; notice the generally steep patterns except for one sample with enriched HREE pattern.

5.3. $^{207}Pb/^{206}Pb$ evaporation data

Based on the morphological (Table 3) and internal features (Fig. 5), representative whole grains were selected for Pb–Pb analyses. To obtain the crystallization age, reproducible $^{207}Pb/^{206}Pb$ ages for different temperature steps of a given grain and robust-consistent ages for different grains from the same sample are needed. Zircon cores characteristically yield increasingly higher $^{207}Pb/^{206}Pb$ ages during higher temperature evaporation. In contrast, grains that have lost radiogenic Pb yield varying young $^{207}Pb/^{206}Pb$ ages as compared to the reproducible $^{207}Pb/^{206}Pb$ crystallization ages from zircon whole grains or fragments that have not lost Pb. Many grains from the same sample were therefore analyzed to place effective $^{207}Pb/^{206}Pb$ constraints on the crystallization age.

Evaporated zircons (ten grains from sample S24, seven from sample S29, eleven from sample S248, and five from sample S112; Table 4), yielded a series of $^{207}Pb/^{206}Pb$ apparent ages that range between 2200 Ma and 2800 Ma. Four grains from sample S24 yielded similar $^{207}Pb/^{206}Pb$ ratios from various evaporation steps. The corresponding age data range between 2717 ± 9 Ma and 2724 ± 3 Ma. All these ages are identical within error, suggesting a common crystallization time. They give a weighted mean age of 2722.7 ± 2.9 Ma (Table 4, Fig. 6a). On the other hand, five other grains yielded heterogeneous $^{207}Pb/^{206}Pb$ ratios from the various temperature steps. Most of the ages are younger than the reproducible ages from the four grains above (2507 ± 4 Ma to 2710 ± 2 Ma) except for two (2720 ± 4 Ma and 2722 ± 3 Ma from the highest temperature step) from grains one and six.

Stable ion beams were achieved only at the last two higher temperature steps from the seven grains from sample S29, except for one grain. Ten apparent ages range from 2218 ± 4 Ma to 2566 ± 7 Ma. Two oldest ages are identical and give a mean age of 2565.9 ± 6.4 Ma.

Table 3
Typologic % distribution of zircons from the Sangmelima high-K granites.

% distribution	0–2%	2–5%	5–10%	10–20%
Typology	S_1, S_7, S_{12}, S_{25}, P_4, D, Ab_1	P_5, Ab_2, Ab_3	S_9, S_{14}, S_{19}, S_{24}	P_2, P_3, S_{10}, S_{15}

Please cite this article as: Shang, C.K., et al., Late Archaean high-K granite geochronology of the northern metacratonic margin of the Archaean Congo craton, Southern Cameroon: Evidence..., Gondwana Research (2010), doi:10.1016/j.gr.2010.02.008

Fig. 5. Cathodoluminescence (CL) and backscattered (BS) images of polished zircons, showing internal structures of various zircon populations. Zircons from sample S24 show smooth relatively intact zircons, while sample S29 zircon crystals show dissolved relicts of CL bright oscillatory zones. Samples S13, S112 and S248 zircons show metamict domains, fractured but unaltered grains, and magmatic oscillatory zoning.

Eleven zircon grains from sample S248 were analyzed. Similar $^{207}Pb/^{206}Pb$ ratios obtained from three grains give similar ages ranging between 2720 ± 3.2 Ma and 2722 ± 4 Ma and yield a mean age of 2720.8 ± 2.4 Ma (Table 4, Fig. 6b). The rest of the grains gave varying ages with increasing evaporation temperatures, ranging between 2423 ± 3 and 2788 ± 35 Ma. The two oldest ages (2778 ± 2.1 Ma and 2788 ± 35 Ma) were obtained at the highest evaporation temperature step.

Five zircons analyzed from sample S112 yielded six different ages varying between 2509 Ma and 2175 Ma. Two oldest ages (2496 ± 2.3 Ma and 2509 ± 3.2 Ma) are closely similar. Grain 3 yielded a reverse age trend with temperature: the older age of 2509 Ma was obtained at the lowest temperature step while the younger age of 2386 Ma was obtained at the highest temperature step.

The identical ages from four zircons and two grain domains from sample S24, three zircons and two grain domains from sample S248 give a weighted mean age of 2722 ± 2 Ma, which we interprete as close approximation to the crystallization age.

5.4. U–Pb zircon dilution data

U–Pb isotope dilution analyses (Table 5) were also performed on carefully selected zircon populations. Five zircon fractions were analyzed from sample S24, four from sample S29 and six from sample S248. All fractions plot below the concordia (Fig. 7). The dispersal of data points does not define good discordia (Fig. 7a, b, c). However, each sample gives similar upper and lower intercepts but with large errors and high MSWD values. The discordia calculated for all fifteen zircon fractions gives upper and lower intercept ages of 2746 ± 40 Ma and 289 ± 37 Ma, respectively, MSWD = 493. Discordia calculation for fourteen fractions, excluding fraction S248-4 which has a large error, yields an upper intercept age of 2751 ± 32 Ma and a lower intercept

Please cite this article as: Shang, C.K., et al., Late Archaean high-K granite geochronology of the northern metacratonic margin of the Archaean Congo craton, Southern Cameroon: Evidence..., Gondwana Research (2010), doi:10.1016/j.gr.2010.02.008

Table 4
Zircon $^{207}Pb/^{206}Pb$ evaporation data showing the minimum crystallization age, Pb loss and inheritance.

Sample (a,b,c = temp. Step)	No. of ratios	Th/U ratios	$^{206}Pb/^{204}Pb$ ratios	$^{207}Pb/^{206}Pb$ ratios 2σ error	$^{207}Pb/^{206}Pb$ age (Ma) 2σ error
S24					
S24-1*	649	1.34	8867	0.18726 ± 38	2718.4 ± 5.2
S24-2*	378	0.98	7898	0.18794 ± 42	2724.4 ± 3.4
S24-3*	247	0.78	10,424	0.18777 ± 42	2722.6 ± 4.2
S24-4*	381	1.22	9863	0.18806 ± 42	2725.2 ± 3.2
Mean			MSWD = 2.1		2723.5 ± 4.1
S24-1a	32	1.18	3907	0.17418 ± 81	2598.3 ± 8.0
S24-1b	200	1.64	4854	0.16490 ± 38	2506.5 ± 4.2
S24-1c	61	1.64	6456	0.18040 ± 67	2656.6 ± 6.4
S24-1d*	341	1.19	9901	0.18707 ± 94	2716.7 ± 8.6
S24-2a	256	1.30	6757	0.18413 ± 63	2690.5 ± 6.0
S24-3a	184	0.92	1014	0.18535 ± 33	2701.4 ± 3.4
S24-4	330	0.92	5848	0.18180 ± 12	2670.0 ± 2.0
S24-5a	13	1.24	6993	0.17940 ± 71	2647.4 ± 6.7
S24-5b	557	1.24	7886	0.18626 ± 10	2709.5 ± 1.8
S24-6a	97	1.42	8646	0.18143 ± 66	2666.2 ± 2.4
S24-6b*	106	1.38	9624	0.18749 ± 42	2720.8 ± 3.6
Mean S24*					2722.7 ± 2.9
S29					
S29-11a	131	3.13	1103	0.15526 ± 15	2403.2 ± 8.2
S29-11b	12	3.13	4545	0.17075 ± 15	2565 ± 19
S29-3a	189	0.52	5236	0.15677 ± 22	2424.4 ± 2.9
S29-3b	105	0.53	5263	0.15810 ± 46	2435.4 ± 5.2
S29-3c	315	0.52	5263	0.15742 ± 24	2428.2 ± 3.1
S29-4	170	0.52	1304	0.16760 ± 73	2533.8 ± 7.6
S29-5	264	2.94	1377	0.16303 ± 33	2487.4 ± 3.7
S29-12	116	0.54	5102	0.15740 ± 79	2427.9 ± 8.7
S29-13	189	0.52	1341	0.17082 ± 72	2565.8 ± 7.4
S29-14	76	0.54	1401	0.13929 ± 29	2218.4 ± 4.0
S248					
S248-1*	477	0.88	9986	0.18738 ± 46	2719.4 ± 3.4
S248-2*	247	0.67	10,034	0.18766 ± 38	2721.3 ± 2.8
S248-3*	424	0.98	9849	0.18788 ± 64	2723.5 ± 3.8
Mean			MSWD = 2.1		2721.3 ± 4.6
S248-1a	303	0.81	9709	0.18325 ± 89	2682.6 ± 1.8
S248-1b	78	0.87	1232	0.17663 ± 47	2622 ± 14
S248-1c*	400	0.87	6655	0.18769 ± 46	2722.1 ± 4.4
S248-2a	342	0.63	5435	0.16247 ± 26	2481.6 ± 3.2
S248-2b	152	0.61	1038	0.17774 ± 38	2631.9 ± 3.9
S248-3a	108	0.96	3677	0.17588 ± 48	2614.5 ± 4.9
S248-3b	302	0.99	3460	0.17446 ± 29	2600.9 ± 3.2
S248-3c	37	0.83	5376	0.18271 ± 33	2678 ± 12
S248-4a	226	1.45	1543	0.15690 ± 23	2422.6 ± 3.0
S248-5a	281	0.99	2778	0.16543 ± 76	2512.0 ± 7.9
S248-5b	104	0.96	3667	0.17349 ± 42	2591.6 ± 4.3
S248-5c	149	0.92	6546	0.18347 ± 73	2684.6 ± 6.8
S248-5d	342	0.79	8547	0.19418 ± 16	2778.0 ± 2.1
S248-6a	192	0.68	4167	0.18394 ± 25	2688.8 ± 2.7
S248-6b	44	0.78	6687	0.19543 ± 13	2788 ± 35
S248-7a	299	1.01	5714	0.18053 ± 23	2657.7 ± 2.7
S248-8a	146	0.78	8767	0.18308 ± 54	2681.4 ± 2.6
S248-8b*	461	0.75	9122	0.18748 ± 44	2720.6 ± 3.2
Mean S248*					2721.2 ± 1.5
S 112					
S112-1	132	0.46	6329	0.14996 ± 42	2345.5 ± 5.1
S112-2	111	0.36	41,667	0.16387 ± 16	2496.1 ± 2.3
S112-3a	134	0.44	7463	0.16510 ± 18	2509 ± 3.2
S112-3b	152	0.44	6667	0.15360 ± 12	2386 ± 2.7
S112-6a	34	0.89	7299	0.13589 ± 81	2175 ± 11
S112-7a	529	1.16	6135	0.14623 ± 56	2302.3 ± 1.7
Mean all*			MSWD = 1.4		2721.9 ± 1.5

*Zircon data with little or no Pb-loss, giving minimum crystallization age.

age of 300 ± 29 Ma, MSWD = 507 (Fig. 7). $^{206}Pb/^{238}U$, $^{207}Pb/^{235}U$, and $^{207}Pb/^{206}Pb$ apparent ages range from 558 ± 3 Ma to 2641 ± 3 Ma, all being younger than the upper intercept age. They suggest that the discordant nature of the fractions is principally a Pb-loss signature without significant influence of inherited zircon cores. The degree of discordance calculated using apparent $^{207}Pb/^{206}Pb$ ages and the lower intercept age of ~300 Ma is highest for sample S248 (69–81%), 70–74% for sample S29, and 49–53% for sample S24 (Table 5).

5.5. Th/U ratios, U–Pb concentrations

Th/U ratios (Tables 4 and 5) were calculated from zircon Pb–Pb evaporation data and from U–Pb isotope dilution data using radiogenic $^{206}Pb/^{208}Pb$ ratios and the inferred crystallization ages. Variations observed from one evaporation temperature step to another for the same zircon grain (Table 4) reflect compositional zoning. Th/U ratios vary from 0.92 to 2.8 for sample S24, from 0.52 to 3.12 for sample S29, from 0.61 to 1.45 for sample S248, and from 0.36 to 1.16 for sample S112. The average Th/U ratios from evaporation data correspond to the ratios determined from the U–Pb data. For comparison, whole-rock ratios show a large variation between 1.1 and 95 (Table 2).

Pb and U concentrations of the zircons were determined from isotope dilution analyses (Table 5). Total Pb concentrations range from 119 to 400 ppm, with common Pb concentrations of 24 to 95 ppm, giving common Pb contents between 12 and 26%. U concentrations of 411 ppm to 618 ppm, 806 ppm to 1359 ppm, and 1269 to 1574 ppm were measured from samples S24, S248, and S29, respectively. Fig. 8 shows the relationship between Th/U ratio, $^{206}Pb/^{238}U$ age, and U content. Data from each sample define a specific field. Comparison of the U concentration and ages (Tables 4 and 5), show that grains with higher U concentrations yield younger ages.

5.6. Sm–Nd and Rb–Sr isotope systematics

Whole-rock Sm–Nd and Rb–Sr isotope data (Table 6) represent the composition of one syenogranite sample (S67) and four monzogranite samples. Nd single stage evolution model ages (T_{DM}) vary from 3040 to 3250 Ma and T_{CHUR} ages are slightly younger (2880 to 3120 Ma). Sm–Nd data yield an errorchron of 2550 ± 780 Ma, MSWD = 4.1, and an initial Nd value of 0.50900 ± 0.00044 (Fig. 9a). ε_{Nd} values calculated for the mean zircon age of 2722 Ma gives crustal values of −2.5 to −5.3. Rb–Sr data give a regression line age of 2557 ± 260 Ma, MSWD = 2.1, with an initial $^{87}Sr/^{86}Sr$ ratio of 0.7089 ± 0.0052 (Fig. 9b). $^{87}Sr/^{86}Sr$ initial ratios calculated for the zircon age of 2722 Ma yield values ranging from 0.70035 to 0.70686, while corresponding ε_{Sr} values range from −12 to 81.

6. Discussion

6.1. Geochemisty

Shang et al. (2007) have shown that Sangmelima high-K granites are generated from the remelting of TTGs and charnockites. The occurrence of such granitic melts shows that critical melt fractions of about 30–40% were attained. Such proportions are required for an acid melt to separate from its source and define discrete magma bodies (e.g. Wickham 1987). This has been estimated for the origin of high-K felsic rocks in California (e.g. Tepper et al., 1993; Borg and Clynne, 1998), which are of similar chemical composition to the Sangmelima high-K granites. Their alkalic to calcic (Fig. 3g) and highly magnesian to highly ferroan (Fig. 3h) compositions are similar to peraluminous leucogranites, although some of their members are less siliceous. They also share partial features of A-type and cordilleran-type granitoids (e.g. Frost et al., 2001). Magnesian and ferroan compositions probably show the interchanging conditions during partial melting of the protolith and conditions under which these various high-K granites crystallized. Magnesian compositions are often characteristic of relatively oxidizing differentiation trends with minor Fe enrichment, and generally mark arc or post-collisional magmas or melts derived from earlier arc magmas (e.g. Frost and O'Nions, 1985). Ferroan composition on the other hand often defines Fe-rich rocks that have

Please cite this article as: Shang, C.K., et al., Late Archaean high-K granite geochronology of the northern metacratonic margin of the Archaean Congo craton, Southern Cameroon: Evidence..., Gondwana Research (2010), doi:10.1016/j.gr.2010.02.008

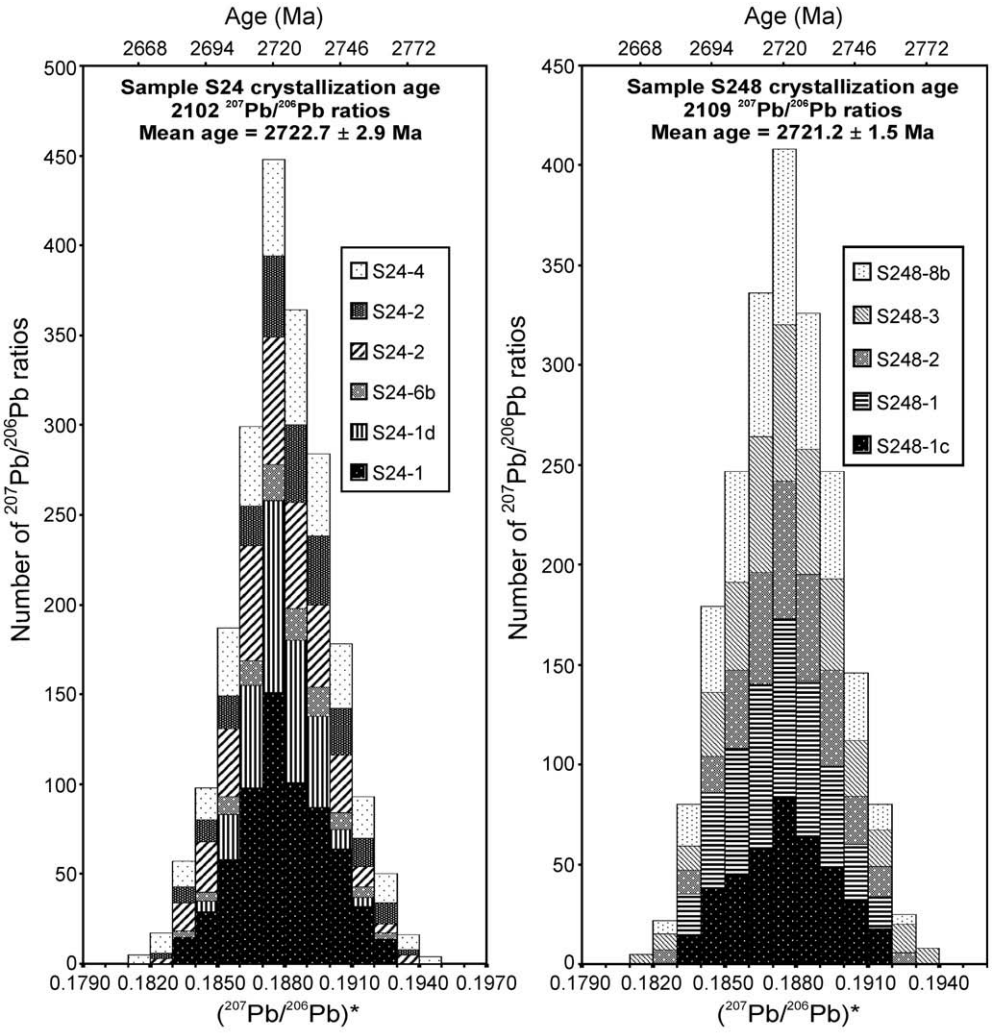

Fig. 6. Histograms showing Gaussian distribution of $^{207}Pb/^{206}Pb$ ratios and mean ages of (a) 2722.7 ± 2.9 Ma for six zircons from sample S24, and (b) 2721.2 ± 1.5 Ma for five zircons from sample S248, interpreted as minimum crystallization ages.

Table 5
Zircon U–Pb analytical data corrected for common Pb according to the two stage evolution model of Stacey and Kramers (1975).

Sample/ sample fraction	Sample weight in mg*	$^{206}Pb/^{204}Pb$	U (ppm)	Pb (ppm)	Pb_{rad} (ppm)	Pb_{com} (ppm)	Pb_{com} in %	Th/U	$^{208}Pb^*/^{206}Pb^*$	Atomic ratios $^{206}Pb/^{238}U$	Atomic ratios $^{207}Pb/^{235}U$	Correlation coefficient	Calculated apparent ages (Ma) $^{207}Pb^*/^{206}Pb^*$	Degree of discordance in %	$^{206}Pb^*/^{238}U$	$^{207}Pb^*/^{235}U$	$^{207}Pb^*/^{206}Pb^*$
Sample S24																	
S24-1	0.020	302.0	411	178	155	23	13	1.8	0.51815	0.2585 ± 15	6.208 ± 38	0.95	0.17416 ± 32	49.4	1482	2006	2598
S24-2	0.020	224.5	618	300	261	39	13	2.7	0.77482	0.2509 ± 15	6.135 ± 38	0.95	0.17738 ± 24	51.7	1443	1995	2629
S24-3	0.027	231.0	526	272	238	34	12	2.8	0.80889	0.2637 ± 15	6.480 ± 37	0.95	0.17824 ± 23	49.2	1509	2043	2637
S24-4	0.014	190.8	598	279	236	43	15	2.4	0.71034	0.2421 ± 13	5.803 ± 35	0.95	0.17394 ± 39	52.7	1398	1947	2595
S24-5	0.030	279.0	560	252	223	29	12	1.9	0.56374	0.2645 ± 14	6.517 ± 36	0.95	0.17870 ± 20	49.1	1513	2048	2641
Sample S29																	
S29-1	0.025	151.0	1574	400	313	87	22	1.7	0.48989	0.1409 ± 73	2.863 ± 16	0.95	0.14737 ± 20	70.2	850	1372	2316
S29-2	0.022	160.5	1269	286	230	57	20	1.9	0.55367	0.1236 ± 06	2.452 ± 14	0.95	0.14381 ± 24	73.8	752	1258	2274
S29-4	0.040	125.2	1330	392	304	89	26	2.6	0.76846	0.1381 ± 07	2.842 ± 16	0.95	0.14923 ± 21	71.1	834	1367	2337
S29-5	0.056	119.2	1545	397	302	95	24	2.6	0.74653	0.1202 ± 07	2.296 ± 13	0.95	0.13858 ± 21	73.9	732	1211	2210
SampleS248																	
S248-1	0.015	272.5	891	199	165	34	17	1.0	0.28171	0.1552 ± 10	3.385 ± 23	0.95	0.15819 ± 34	68.6	930	1501	2437
S248-2	0.027	148.7	1182	180	142	38	21	1.2	0.34266	0.0904 ± 05	1.701 ± 10	0.95	0.13639 ± 32	81.3	558	1009	2182
S248-3	0.017	223.8	1277	181	147	34	19	0.8	0.23635	0.0985 ± 05	1.765 ± 10	0.95	0.13001 ± 23	78.3	605	1033	2098
S248-4	0.024	285.0	974	171	140	31	18	1.0	0.27793	0.1220 ± 29	2.706 ± 64	0.95	0.16087 ± 15	76.4	742	1330	2465
S248-5	0.022	212.6	1359	242	202	40	17	1.4	0.40817	0.1115 ± 07	2.132 ± 13	0.95	0.13865 ± 22	76.1	682	1159	2210
S248-6	0.043	182.1	806	119	95	24	20	1.1	0.32404	0.0940 ± 06	1.757 ± 12	0.95	0.13555 ± 22	80.2	576	1030	2171

All errors quoted are 2σ absolute uncertainties and refer to the last digit.
* = radiogenic ; grain size varies from 80 to 180 μm.
mg* = error in weight is estimated to be up to 10%.

Please cite this article as: Shang, C.K., et al., Late Archaean high-K granite geochronology of the northern metacratonic margin of the Archaean Congo craton, Southern Cameroon: Evidence..., Gondwana Research (2010), doi:10.1016/j.gr.2010.02.008

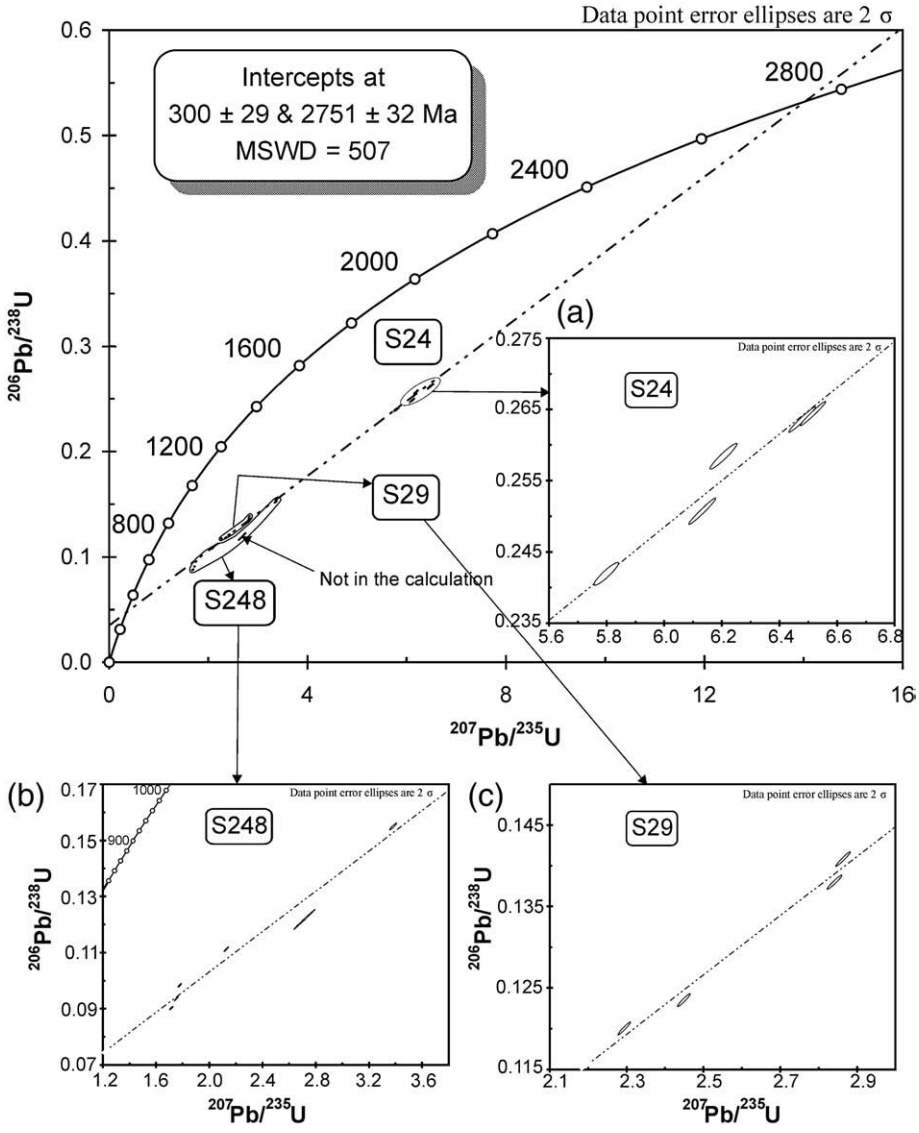

Fig. 7. U–Pb discordia diagrams for six zircon fractions from sample S248, five fractions from sample S24 and four fractions from sample S29. Scattering of data points define a discordia band, yielding an upper intercept age of 2751 ± 32 Ma and a lower intercept of 300 ± 29 Ma. All fractions indicate radiogenic Pb-loss with high percentage discordances ranging between 49% and 81%.

undergone extensive fractionation at low oxygen fugacity. They are often evolved magmas characteristic of intraplate environments (e.g. Duchesne and Wilmart, 1997).

Subduction signatures (negative Nb and Ti anomalies (Fig. 4a), and negative Ta anomaly not shown) are interpreted as source TTG and charnockite inherited features. The negative and positive Eu anomaly variation (Fig. 4b) may indicate melting under low and high water activity, respectively. If the relatively high Y and Yb contents of some samples and their almost flat REE pattern are suggestive of a garnet-free source, then it is likely that partial melting was under low pressure within the middle of the crust. Garnet is often absent in dehydration melting experiments conducted at less than 8 kbar (e.g. Rushmer, 1991; Rapp et al., 1991). However, the low concentration in Ti and Yb and the high La_N/Yb_N and Gd_N/Yb_N ratios reflected in the steeper REE patterns of some samples (Fig. 4b) could be due to a garnet-rich residue (e.g. Kay et al., 1994; Mpodozis et al., 1995; Kay and Abbruzzi, 1996). The presence of garnet would suppose pressures of >10 kbar (e.g. Wolf and Wyllie, 1994).

6.2. Implications from geochronologic and isotopic data

U–Pb isotope dilution data are very discordant and dispersed. They define a discordia band with an upper intercept at 2751 ± 32 Ma and a lower intercept at 300 ± 29 Ma, MSWD = 507 (Fig. 7). Despite being characterized by a high MSWD value, this discordia band is completely different from a cloud distribution and can be interpreted as the result of lead loss affecting the zircons initially defining an age range. The lower intercept (300 ± 29 Ma) can be interpreted either as a Variscan orogenic effect or as a mixed age between the Pan-African orogeny and recent lead losses. $^{206}Pb/^{238}U$ apparent ages (Table 5) do show Pan-African (Neoproterozoic) ages (558–930 Ma) while the $^{207}Pb/^{206}Pb$ apparent ages especially for sample S29 and S248 (Table 5) record Eburnean (Early Proterozoic) ages (2098–2465 Ma), and Pb evaporation data from samples S29 and S112 (Table 4) do again give Eburnean ages (2178–2487 Ma). However, discordia plots for $^{206}Pb/^{238}U$ and $^{207}Pb/^{235}U$ data yield only Archaean upper intercept ages (Fig. 7), thereby excluding the interpretation of Eburnean crystallized zircon. But the Eburnean tectonothermal effect on the Ntem complex

Please cite this article as: Shang, C.K., et al., Late Archaean high-K granite geochronology of the northern metacratonic margin of the Archaean Congo craton, Southern Cameroon: Evidence..., Gondwana Research (2010), doi:10.1016/j.gr.2010.02.008

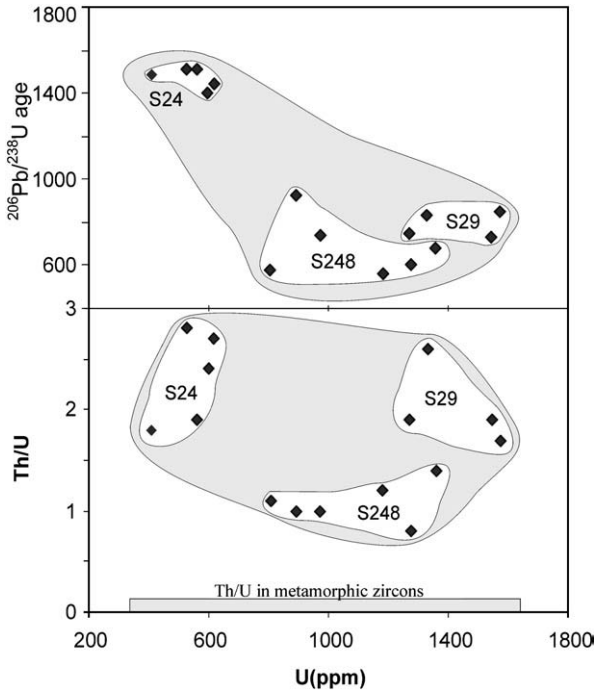

Fig. 8. Plots showing the $^{206}Pb/^{238}U$ age, Th/U and U content of zircon fractions from three high-K granite samples: (a) $^{206}Pb/^{238}U$ ages as a function of U content. The negative correlation indicates Pb-loss controlled by U radiation damage, with U-rich fractions more affected; (b) characteristic magmatic zircon Th/U ratios versus U concentration.

has been documented by Rb–Sr biotite ages (Shang et al., 2004a). This suggests that the tectonothermal effect of this orogeny at this part of the Archaean Congo craton probably attained only the comparatively low biotite recrystallization and/or Rb–Sr reset temperature (~300 °C; Harrison et al., 1985; Dodson and McClellan-Brown, 1985) and not the high zircon recrystallization and/or U–Pb reset temperature (>900 °C; Mezger, 1990; Cherniak and Watson, 2001; Cherniak et al., 2004). Considering the regional geology that is characterized by the overthrusting Pan-African mobile belt onto the Archaean Congo craton and geochronologic history (Fig. 1; Toteu et al., 2001, 2006 and references therein; Mvondo et al., 2003), we favour the hypothesis of Pan-African orogeny and recent lead loss. Pan-African episodic imprints marked by Archaean zircon U–Pb lower intercept ages of 560–640 Ma have widely been reported from charnockitic and TTG formations of the Ntem complex (Toteu et al., 1994; Feybesse et al., 2008; Shang et al., 2004b; Takam et al., 2009). This strong Pan-African imprint is however not preserved in all the analyzed zircons (e.g. Shang et al., 2004b) including the high-K granite zircons in this study with a lower intercept age of 300 ± 29 Ma (Fig. 7). This is surprisingly a Variscan age, whereas Variscan events are not known in the study area. Only Pan-African zircon U–Pb lower intercept ages, as mentioned above, have so far been reported in the Ntem complex. Other non-Archaean events recorded by Eburnean zircon growth and titanite ages have been identified in the Lower Nyong metagranitoids (Toteu et al., 1994; Lerouge et al., 2006) at the northwestern border of the Ntem complex (Fig. 1). Eburnean effect in the study area is recorded only by the biotite Rb–Sr system (Shang et al., 2004a). As a result, we interpret the ca. 300 Ma lower intercept age as the mean of several events, including continuous diffusion and leaching, and partial resetting of the U–Pb system (Corfu and Ayres, 1984; Mezger and Krogstad, 1997; Corfu, 2000; Kramers et al., 2009) that have affected the region since the Pan-African orogenic symmetric age of 600 Ma.

The fact that no Pan-African Rb–Sr biotite ages are recorded suggests that Pan-African orogenic effect in the study area was colder than the Eburnean effect, resulting in more brittle deformation that favoured aqueous fluid circulation and leaching. Low temperature zircon alteration, leaching and Pb-loss paradox is widely reported (Corfu and Ayres, 1984; Mezger and Krogstad, 1997; Corfu, 2000; Kramers et al., 2009). Brittle deformation of the study area was therefore more intensely enhanced by the effect of the Pan-African orogeny than by the effect of the Eburnean orogeny.

$^{207}Pb/^{206}Pb$ evaporation data gave a wide range of ages (2218 ± 4 Ma to 2788 ± 35 Ma; Table 4) from the various temperature steps. Zircons from samples S24 and S248 yielded generally older $^{207}Pb/^{206}Pb$ ages than those obtained from samples S29 and S112. Considering the internal structure of the zircons (Fig. 5), we interpret most of the Pb evaporation data to represent various degrees of Pb-loss. CL and backscattered images (Fig. 5) show fractured and metamict zircon structures, inherent indicators that favour radiogenic Pb-loss. These evaporation data are therefore most probably not concordant. Most of the ages defined by the peaks (Fig. 10a) demonstrate the variability of discordance of the Sangmelima granite zircons that have been affected by much younger events, e.g., the Pan-African orogeny and Phanerozoic events. This implies that the crystallization age of the Sangmelima high-K granites lies among the older $^{207}Pb/^{206}Pb$ evaporation ages obtained at high evaporation temperatures. In fact, the evaporation record generally shows pure radiogenic Pb during the final evaporation steps (e.g. Kober, 1986; Klötzli, 1999; Kramers et al., 2009). Indeed, among the older $^{207}Pb/^{206}Pb$ ages, zircon grains from samples S24 and S248 yielded old identical ages at the high evaporation steps, similar to a series of ages (2717 ± 9 Ma to 2724 ± 3 Ma; Table 4) obtained at various evaporation temperature steps from some zircons. Their $^{207}Pb/^{206}Pb$ ratios are homogeneous, suggesting little or no Pb-loss. Losing the same proportions of ^{206}Pb and ^{207}Pb in zircon grains affected by subrecent Pb leaching with an "accessibility ratio" between 1.14 and 1.29 could equally give such homogeneous $^{207}Pb/^{206}Pb$ ratios (e.g. Kramers et al., 2009). Consequently, we interpret this set of similar $^{207}Pb/^{206}Pb$ ages as marking minimum crystallization time. The fact that these ages from the middle and high evaporation steps are from some grains that yielded varying $^{207}Pb/^{206}Pb$ ratios (Table 4) indicates that some of these zircon domains might have conserved most or all of their radiogenic Pb and can thus effectively constrain the crystallization age, even though neighboring sectors lost radiogenic Pb (e.g. Hanski et al., 2005; Kramers et al., 2009). The mean of these ages (2721.9 ± 1.5 Ma) characterized by the highest peak in Fig. 10a is interpreted as the best mean approximation of the minimum crystallization age of the high-K granites in the Sangmelima region. Other high peaks in Fig. 10a are

Table 6
Sm, Nd, Rb and Sr abundances and isotopic composition from Sangmelima high-K granitic suite.

	Sample	Sm	Nd	$^{147}Sm/^{144}Nd$	$^{143}Nd/^{144}Nd \pm 2\sigma_m$	εNd_{2722Ma}	T_{DM}/Ma	T_{CHUR}/Ma	Rb ppm	Sr ppm	$^{87}Rb/^{86}Sr$	$^{87}Sr/^{86}Sr \pm 2\sigma_m$	$Sr_{2722\ Ma}$	$\varepsilon Sr_{2722\ Ma}$
Granitic suite members	S24	6.926	66.1	0.0636	0.510072 (7)	−3.4	3037	2914	128.0	414.0	0.898	0.742223 (10)	0.70685	80
	S26	4.284	23.4	0.1106	0.510904 (8)	−3.7	3210	3052	239.7	209.0	3.360	0.836486 (10)	0.70407	41
	S29	6.637	53.5	0.0751	0.510327 (10)	−2.5	3011	2876	128.5	157.3	2.384	0.794286 (10)	0.70035	-12
	S31	1.367	8.75	0.0944	0.510532 (7)	−5.3	3251	3117	118.0	297.0	1.155	0.752360 (12)	0.70686	81
	S67	0.336	2.58	0.0787	0.510289 (10)	−2.7	3142	3015	186.0	412.0	1.312	0.756330 (10)	0.70461	49

$_m$ error of measured value.

Please cite this article as: Shang, C.K., et al., Late Archaean high-K granite geochronology of the northern metacratonic margin of the Archaean Congo craton, Southern Cameroon: Evidence..., Gondwana Research (2010), doi:10.1016/j.gr.2010.02.008

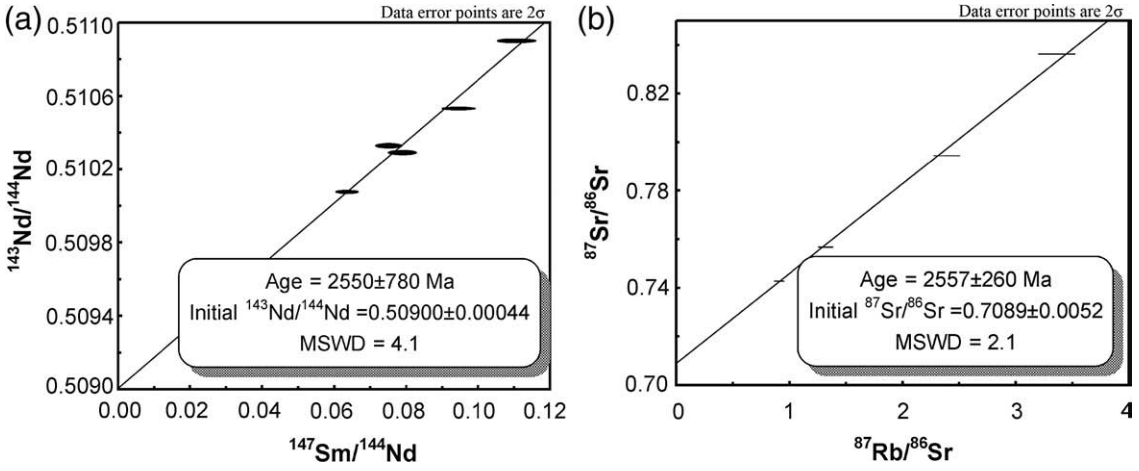

Fig. 9. (a) Sm/Nd and (b) Rb/Sr Nicolaysen diagrams. Both errorchron ages are similar within error but large error values indicate the disturbed nature of the both isotopic systems.

defined between 2660 Ma and 2710 Ma. The lower limit of this age range is similar to the age of high-K granitoids from the Ebolowa region of the Archaean Congo craton (2666 ± 2 Ma; e.g. Tchameni et al., 2000). An additional higher peak at 2778 ± 4 Ma generates a wide age vacuum (WAV) of more than 50 My with the crystallization age. This $^{207}Pb/^{206}Pb$ crystallization age agrees with the upper intercept

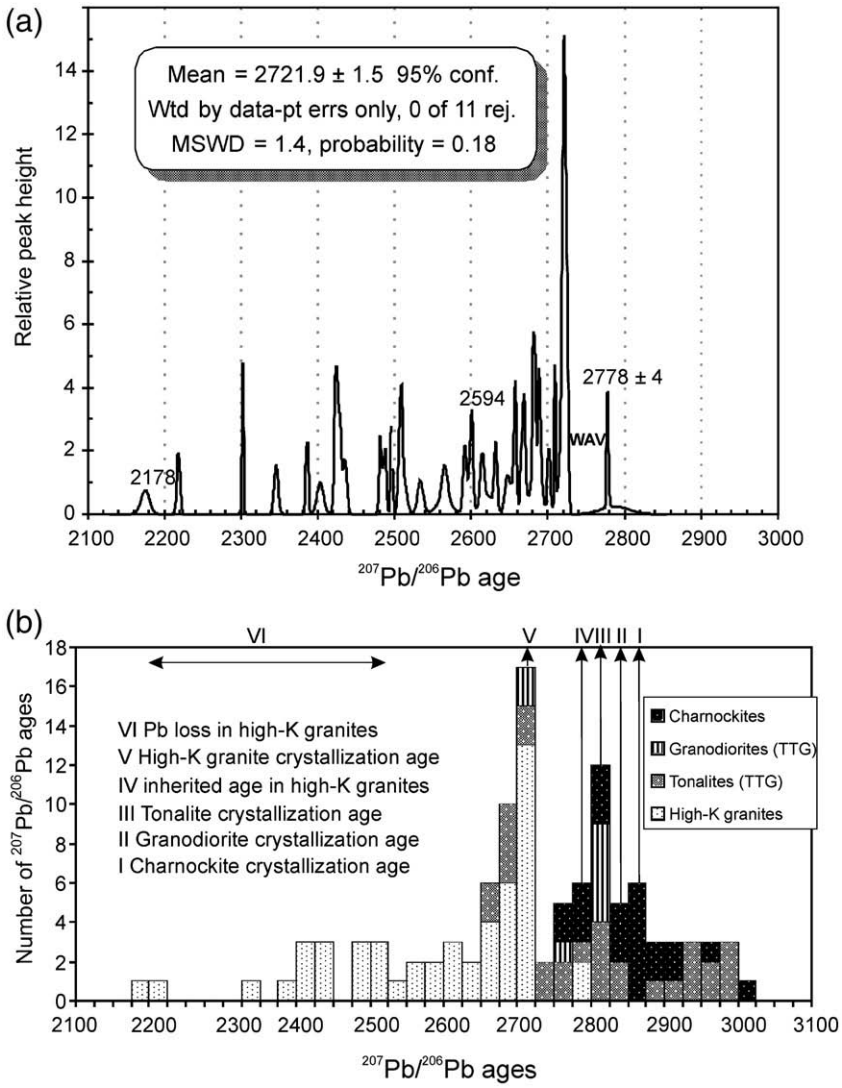

Fig. 10. Zircon $^{207}Pb/^{206}Pb$ evaporation age data: (a) spatial distribution of $^{207}Pb/^{206}Pb$ evaporation ages in high-K granites; note the wide age vacuum (WAV) that marks the time lapse between crystallization time and old inherited ages; (b) histogram comparing $^{207}Pb/^{206}Pb$ zircon age distribution in high-K granite to $^{207}Pb/^{206}Pb$ zircon age distribution in host/source rocks (TTGs and charnockites; Shang et al., 2004b).

Please cite this article as: Shang, C.K., et al., Late Archaean high-K granite geochronology of the northern metacratonic margin of the Archaean Congo craton, Southern Cameroon: Evidence..., Gondwana Research (2010), doi:10.1016/j.gr.2010.02.008

of the multi-grain conventional U–Pb dilution age of 2751 ± 32 Ma. This implies that the oldest ages measured (2778 ± 4 Ma and 2788 ± 35 Ma; Table 4) must be considered as belonging to zircon parts [influenced by zircon cores] inherited from the source rocks of the high-K granitoids. It is difficult to determine if this age actually corresponds to that of the source or is a minimum age for the source, Pb-loss being possible at the time of source melting. Taking the conservative view, we interpret the age of 2778 ± 4 Ma as a minimum age for the source of the Sangmelima high-K granitoids. The local granodiorite (TTG) and charnockite crystallization ages have been set to 2834 ± 4 Ma and 2884 ± 10 Ma, respectively (e.g. Shang et al., 2004b; Pouclet et al., 2007). The inherited zircon in the high-K granitoids could then come from the TTG or charnockite source.

A comparison of high-K granite zircon evaporation age data in this paper and TTG and charnockite zircon evaporation age data from Shang et al. (2004b) is graphically presented in Fig. 10b. High-K granite evaporation age data pattern marked by inheritance, crystallization, and reset ages are similar to age distribution patterns in TTG and charnockites. This age distribution pattern indicates differentiation of the Ntem crust since its formation from basic protocrust (>3100 Ma; Shang et al., 2004a). The melting of the protocrust occurred in a subduction setting and resulted in charnockite and TTG emplacement (e.g. Shang et al., 2004a). The charnockite and TTG crust then differentiated in late Archaean times generating high-K granites (e.g. Shang et al., 2007). This crustal differentiation is marked by continuous transfer of material characterized by inheritance and resetting of Pb–Pb ages throughout Archaean times. Granitoid zircons from the Ntem complex therefore bear benchmarks of crustal evolution in the Archaean Congo craton.

Rb–Sr and Sm–Nd whole-rock ages in this study are marked by large errors (2557 ± 260 Ma, 2550 ± 780 Ma; Fig. 9). These ages encompass all Archaean and Palaeoproterozoic ages measured by the U–Pb and Pb–Pb zircon methods. They further indicate the intensely disturbed radiometric systems at the northern border of the Archaean Congo craton. However, initial Sr ratios calculated for the zircon age ($Sr_{i.2722\ Ma}$ 0.7004 and 0.7069) and epsilon Sr values ($\varepsilon_{Sr\cdot 2722\ Ma}$ −12 to 81) indicate crustal values and one mantle-like value. $\varepsilon_{Nd\cdot 2722\ Ma}$ values (−2.5 to −5.3) reflect crustal sources. The model ages in this study (3.03–3.25 Ga) are similar to those reported from the TTGs and charnockitic protolith of the high-K granites (Shang, 2001; Shang et al., 2004a, 2007). The lone Sr mantle-like value could be erroneously interpreted as a signature of assimilated amphibolitic xenolith in TTG and charnockite, but it appears to mark alteration than a mantle signature, given the ε_{Nd} crustal value −2.5 from the same sample. Isotope data therefore strongly support the interpretation that the Sangmelima high-K granitoids are derived from TTG and charnockite sources (e.g. Shang et al., 2007), and demonstrate that the high-K magmatic event did not add new mantle material to the crust, but was merely a remelting episode of the pre-existing crust. Doleritic formations of similar age as the high-K granites in the same region have lead to the interpretation that doleritic magmatism constituted the heat source for crustal remelting (e.g. Shang et al., 2007).

6.3. Explaining zircon Pb-loss

The zircon U–Pb chronometer is the most widely used and the most trusted one in Precambrian geochronology, yet the systematics show, time and again, puzzling features. The strong retentivity of radiogenic Pb in zircons at high-grade temperatures and in melts is well known (e.g. Vavra et al., 1996; Bowring and Williams, 1999; Dunn et al., 2005; Pidgeon and Nemchin, 2006; Pidgeon et al., 2007). On the other hand, examples of severe discordance reflecting more than 50% loss of radiogenic Pb are also very common. Whereas high degrees of discordance are widely reported from the African Precambrian, relatively low degrees of discordance are reported from the Canadian Shield or West Greenland Archaean zircons for example (e.g. Bowring and Williams, 1999; Nutman et al., 2004), and much less or no discordance is shown by Lunar zircons, even those with high U-contents (Nemchin et al., 2006; Pidgeon et al., 2007). Discordance is often associated with specific local or regional tectono-metamorphic events, but often too, no such events are evident. As a result it has been suggested that the latter may be caused by groundwater acting on zircon metamict structure (Stern et al., 1966; Black, 1987; Mezger and Krogstad, 1997).

All zircon fractions in this study (Table 5) are characterized by strong discordance of up to 81% in some cases (Fig. 7). Representative CL images of the analyzed zircons, (Fig. 5), show inherent features, (metamict domains and fractures), typical of zircons that have lost radiogenic Pb. Even the evaporation technique, devoted to analyze separately the best preserved parts of the zircons, gave a wide range of ages attributed to discordance due to Pb-loss.

The phenomenon of radiogenic Pb-loss in zircon is well known (e.g. Corfu and Ayres, 1984; Corfu, 2000, Kramers et al., 2009). In zircon U–Pb systematics, extreme robustness up to the temperatures of granulite facies and anatexis contrasts with apparently easy loss of radiogenic Pb at low temperatures. Pb-loss often occurs by diffusion and leaching, more likely as a result of discrete tectono-metamorphic events with increased heat flow and fluid movements, and possibly too as a continuous process after tectonic phases, or even during uplift and surface weathering, often without any metamorphic event being in evidence. Kramers et al. (2009) propose that this paradoxical behaviour can be understood with the hypothesis that radiogenic Pb in zircon is tetravalent. These authors argue that radiogenic Pb should be tetravalent based on analogies with studies relating to the tetravalent state of ^{234}Th and the hexavalent state of ^{234}U (Ordonez Regil et al., 1989; Adloff and Roessler, 1990), which show that α-recoil in silicates generates a strongly oxidizing environment at the site where the recoiling nucleus comes to rest. They further propose that a zircon grain, being small, should remain highly oxidizing in its interior by the constant loss of β-particles, maintaining the 4+ state of radiogenic Pb. Kober (1987) suggested that radiogenic Pb should be tetravalent, which would make it compatible in the zircon lattice. From its effective ion radius, similar to that of Zr^{4+}, and its charge, Pb^{4+} can substitute even better for Zr than U or Th, thus thought to be highly compatible in the zircon lattice (Frei et al., 1997; Kramers et al., 2009). Furthermore, the activation energies for the tetravalent ions of U, Th and Hf in zircon are very much higher than for divalent Pb, (Cherniak et al., 1997a, b), and lead to diffusivities that are about 3 orders of magnitude lower than that for divalent Pb in zircon. By analogy, Kramers et al. (2009) argue that tetravalent Pb, being similar in effective ion radius and charge to U, Th, and Hf, would have similarly low diffusivities. On the account of these factors, extreme retentivity of U–Pb clocks even at high temperatures could then be understood (Kramers et al., 2009). It also then follows that radiogenic lead cannot be lost from zircon crystals except by being reduced to the divalent state, after which it would become both incompatible in the lattice and highly mobile in solution. Cherniak et al. (1997a, b) have shown that radiogenic Pb situated in α-recoil damaged sites (metamict domains) is easily reduced by an electrolyte solution to the divalent state, making it both incompatible and soluble and then leached out. As a result, it is thought that not only hydrothermal fluids, but also natural leaching by groundwater in weathering can both reduce the Pb to the divalent state, and transport it (Kramers et al., 2009). In fact, numerous observations on natural cases of discordance of zircon dates (Stern et al., 1966; Black, 1987; Mezger and Krogstad, 1997), as well as leaching experiments (Hansen and Friderichsen, 1989; Sinha et al., 1992; Frei and Kamber, 1995; Frei et al., 1997; Mattinson, 1994, 2000; Davis and Krogh, 2000), illustrate this. Consequently, it is now generally accepted that the discordance of many zircon U–Pb data sets is due to deep groundwater interaction related to weathering, even in cases where the rock does not appear altered. This typically applies to Precambrian

Please cite this article as: Shang, C.K., et al., Late Archaean high-K granite geochronology of the northern metacratonic margin of the Archaean Congo craton, Southern Cameroon: Evidence..., Gondwana Research (2010), doi:10.1016/j.gr.2010.02.008

suites with reasonably precise upper concordia intercepts, and poorly defined lower intercepts that cannot be accounted for by any known metamorphic episode (e.g. Kröner et al., 1999). Typical examples are mostly located in areas of deep tropical weathering or palaeoweathering (Kramers et al., 2009), such as the Limpopo Belt in southern Africa (Kröner et al., 1999), and the Ntem complex in southern Cameroon as shown in this study.

6.4. Ntem complex–Pan-African metacratonization connection

The metacraton concept (Abdelsalam et al., 2002), refers to a geologic situation where a cratonic basement is reactivated, so that it neither behaves as a stable craton nor as a classical mobile belt. It does not again retain all the qualities of a stable craton. Instead, the basement is characterized by either intense metamorphism or granitoid magmatism or deformation or any comibation of all these.

Pan-African events of the Archaean Ntem complex, marked by deformation (fragile tectonics) and dircordant zircon U–Pb lower intercept ages (Toteu et al., 1994; Shang et al., 2004b; Takam et al., 2009), are thought to be caused by the collisional impact with the overthrusting Central African fold belt (Fig. 1; Maurizot et al., 1986; Toteu et al., 1994; Shang et al., 2004b; Takam et al., 2009). This northern margin of the Archaean Congo craton has been subducted during the collision with the Pan-African orogenic belt before being exhumed together with the Yaounde nappes (e.g. Toteu et al., 2001, 2006). Such an event has the potential to reactivate the subducted part, which is corresponding to a metacratonization process (e.g. Liégeois et al., 2003). This suggests that the Ntem complex represents the northern metacratonic boundary of the Archaean Congo craton, thus being a partly destabilized segment of the Congo craton that has retained only some cratonic characteristics (e.g. Abdelsalam et al., 2002; Liégeois et al., 2003).

Metacratonization favours fluid or magma passage, which can chemically affect the basement rocks including the zircons. However, the zircon Th/U ratios of 0.36–3.12 (Tables 4 and 5) are in the typical range of magmatic zircons, being much higher than in metamorphic zircons (<0.3; e.g. Kröner et al., 1994; Klötzli-Chowanetz et al., 1997; Klötzli, 1999; Whitehouse et al., 1999; Rubatto and Gebauer, 2000; Rubatto, 2002; Möller et al., 2002). This indicates that Pan-African metacratonization of the northern border of the Archaean Congo craton was not a metamorphic event, and confirm U–Pb lower intercept ages as due to Pb-loss and not to metamorphic zircon growth.

Zircons from the Sangmelima high-K granites could have thus lost radiogenic Pb during the Pan-African orogeny due to hydrothermal fluid circulation through fractures and shear zones activated during the Pan-African thrusting event. These rigid but fractured metacratonic areas are particularly susceptible to reactivation when stress is applied elsewhere on the plate (e.g. Azzouni-Sekkal et al., 2003; Liégeois et al., 2005; Ennih and Liégeois, 2008). This was probably the case for this northern boundary of the Archaean Congo craton during the Phanerozoic, with stress coming from the Benue trough rifting process, the opening of the Atlantic, and currently from the active Cameroon volcanic line. The current metacratonic location of the Ntem complex can be modelled with tomographic data (e.g. Fig. 11). The characteristic thick lithosphere of cratonic areas is only evident at the rear of the Ntem area. Although the resolution of the tomographic model is low (about 100 km, Shapiro, written communication, Shapiro, 2004), it is precise enough to demonstrate that the Ntem complex belongs to an intermediate region between the true Archaean Congo craton and the Pan-African mobile belt, actually to the metacratonic boundary of the Congo craton at 600 Ma. The complexity of the zircon U–Pb data can be ascribed to this metacratonic nature of the Ntem complex generated during the Pan-African orogeny and reactivated several times during the Phanerozoic. This shows that relatively robust metacratonic domains are actually very active in terms of trace element mobility, even at microscales. This should be considered during evaluation of economic mineralization potential.

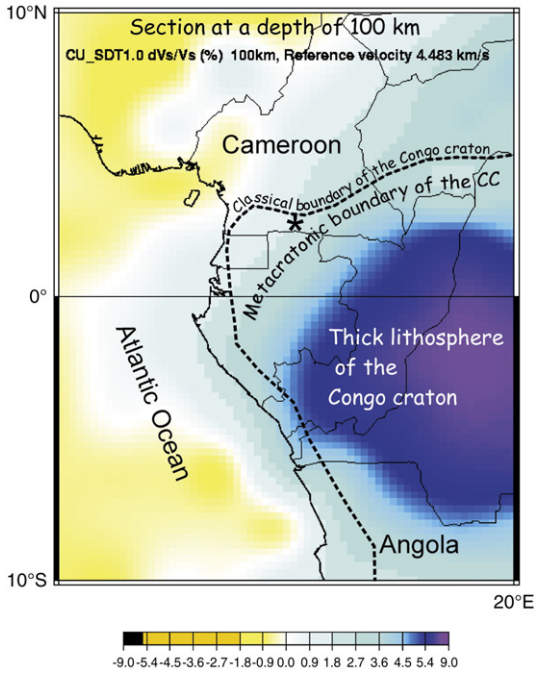

Fig. 11. Central African maps showing 3D shear-wave velocity tomographic model at a depth of 100 km based on surface wave diffraction tomography map generated from the CUB model of N. Shapiro (http://ciei.colorado.edu/~nshapiro/MODEL/); Surface wave diffraction tomography and data processing is described in Ritzwoller et al. (2002) and Shapiro and Ritzwoller (2002). Color scale shows the shear velocity as % perturbation relative to the reference velocity value of 4.483 km/s for a depth of 100 km. The mark (X) indicates the Sangmelima region in the Archaean Congo craton metacratonic margin.

7. Conclusions

Due to radiogenic Pb-loss, high-K granite zircons are strongly discordant (49–81%; isotope dilution bulk technique) or display a wide range of $^{207}Pb/^{206}Pb$ ages (zircon evaporation technique). Th/U ratios of the zircons typically reflect magmatic zircon values. Sr and Nd isotope systematics are identical to those of TTG and charnockites. These results indicate:

(1) The minimum estimate of the crystallization age of the Sangmelima high-K granites is 2722 ± 2 Ma. This age suggests that high-K granite emplacement occurred some ca. 100 My after the main Ntem complex–Archaean Congo craton crustal acrretion process (ca. 2800 to 2900 Ma, e.g. Toteu et al. 1994; Shang et al. 2004b; Pouclet et al., 2007; Takam et al., 2009).
(2) Inherited zircons, aged 2778 ± 4 Ma, mark a minimum age for the granite source rocks. Coupled with similar Nd isotope compositions and identical Nd T_{DM} ages of ca. 3 Ga as TTG, the high-K granitic event in the Sangmelima region added no new juvenile material to the Ntem complex, revealing that this event was merely a differentiation episode of the existing crust.
(3) The complex set of U–Pb ages resulting from significant Pb-loss is a consequence of leaching, enhanced by non-metamorphic events such as the Pan-African metacratonization of the northern boundary of the Archaean Congo craton, later reactivation and uplift during the Phanerozoic. Metacratonic areas are indeed preferential loci for intraplate reactivations (e.g. Liégeois et al., 2005; Ennih and Liégeois, 2008) and trace element remobilization.

Please cite this article as: Shang, C.K., et al., Late Archaean high-K granite geochronology of the northern metacratonic margin of the Archaean Congo craton, Southern Cameroon: Evidence..., Gondwana Research (2010), doi:10.1016/j.gr.2010.02.008

Acknowledgments

The authors are grateful to Elmar Reitter and Christian Dekant for the laboratory assistance. CKS would like to express his indebtedness to St. Paulus and St Johannes Catholic Parishes, Tübingen, for the spiritual up-keep. Special thanks go to Prof. M. Santosh, the Editor in Chief of Gondwana Research, Prof. Guochun Zhao and an anonymous Reviewer for their constructive advice and recommendations that have helped improve our paper. Much gratitude goes to DAAD for the initial support of this research project.

References

Abdelsalam, M., Liégeois, J.P., Stern, R.J., 2002. The Saharan metacraton. Journal of African Earth Sciences 34, 119–136.

Adloff, J.P., Roessler, K., 1990. Recoil and transmutation effects in the migration behaviour of actinides. Radiochimica Acta 52 (53), 269–274.

Appel, P., Schenk, V., Schumann, A., 2005. P–T path and metamorphic ages of pelitic schists at Murschison Falls, NW Uganda: evidence for a Pan-African tectonometamorphic event in the Congo craton. European Journal of Mineralogy 17, 655–664.

Azzouni-Sekkal, A., Liégeois, J.P., Bechiri-Benmerzoug, F., Belaidi-Zinet, S., Bonin, B., 2003. The "Taourirt" magmatic province, a marker of the very end of the Pan-African orogeny in the Tuareg Shield: review of the available data and Sr–Nd isotope evidence. Journal of African Earth Sciences 37, 331–350.

Barbey, P., Macaudière, J., Nzenti, J.P., 1990. High pressure dehydration melting of metapelites: evidence from migmatites of Yaounde (Cameroon). Journal of Petrology 31, 401–427.

Black, L.P., 1987. Recent Pb loss in zircon. A natural or laboratory-induced phenomenon? Chemical Geology (Isotope Geoscience) 65, 25–33.

Borg, L.E., Clynne, M.A., 1998. The petrogenesis of felsic calc-alkaline magmas from the southernmost Cascades, California: origin by partial melting of basaltic lower crust. Journal of Petrology 39, 1197–1222.

Bowring, S.A., Williams, I.S., 1999. Priscoan (4.00–4.03 Ga) orthogneisses from northwestern Canada. Contributions to Mineralogy and Petrology 134, 3–16.

Castaing, C., Feybesse, J.L., Thiéblemont, D., Triboulet, C., Chèvremont, P., 1994. Palaeogeographical reconstructions of the Pan-African/Braziliano orogen: closure of an oceanic domain or intracontinental convergence between major blocks? Precambrian Research 69, 327–344.

Cawood, P.A., Kröner, A., Collins, W.J., Kusky, T.M., Mooney, W.D., Windley, B.F., 2009. Accretionary orogens through Earth history. Geological Society, London, Special Publications 318, 1–36.

Celino, J.J., Botelho, N.F., 2005. Geochemical evolution and petrogenesis of igneous charnockites in the coastal mobile belts of Brazil. Boletim Paranaense de Geociências 57, 25–47 Editora UFPR.

Chen, F., Siebel, W., Satir, M., 2002. Zircon U–Pb and Pb isotope fractionation during stepwise HF-acid leaching and geochronolgical implications. Chemical Geology 191, 155–164.

Cherniak, D.J., Watson, E.B., 2001. Pb diffusion in zircon. Chemical Geology 172, 5–24.

Cherniak, D.J., Hanchar, J.M., Watson, E.B., 1997a. Rare-earth diffusion in zircon. Chemical Geology 134, 289–301.

Cherniak, D.J., Hanchar, J.M., Watson, E.B., 1997b. Diffusion of tetravalent cations in zircon. Contributions to Mineralogy and Petrology 127, 383–390.

Cherniak, D.J., Watson, E.B., Grove, M., Harrison, T.M., 2004. Pb diffusion in monazite: a combined RBS/SIMS study. Geochimica et Cosmochimica Acta 68, 829–840.

Cocherie, A., Guerrot, C., Rossi, P.H., 1992. Single-zircon dating by step-wise Pb evaporation: comparison with other geochronological techniques applied to the Hercynian granites of Corsica, France. Chemical Geology 101, 131–141.

Condie, K.C., 2000. Episodic continental growth models: afterthoughts and extensions. Tectonophysics 322, 153–162.

Condie, K.C., Benn, K., 2006. Archaean geodynamics: similar or different from modern geodynamics. In: Benn, K., Mareschal, J.-C., Condie, K.C. (Eds.), Archaean Geodynamics and Enivironments: American Geophysical Union Washington, DC. Geophysical monograph, 164, pp. 47–59.

Condie, K.C., Belousova, E., Griffin, W.L., Sircombe, K.N., 2009. Granitoid events in space and time: constraints from igenous and detrital zircon age spectra. Gondwana Research 15, 228–242.

Corfu, F., 2000. Extraction of Pb with artificially too-old ages during stepwise dissolution experiments on Archaean zircon. Lithos 53, 279–291.

Corfu, F., Ayres, L.D., 1984. U–Pb ages and genetic significance of heterogeneous zircon populations in rocks from the Favourable Lake area, northwestern Ontario. Contributions to Mineralogy and Petrology 88, 86–101.

Corfu, F., Hanchar, J.M., Hoskin, P.W.O., Kinny, P., 2003. Atlas of zircon textures. In: Hanchar, J.M., Hoskin, P.W.O. (Eds.), zircon: Reviews in Mineralogy and Geochemistry, 53, pp. 469–500.

Davis, D.W., Krogh, T.E., 2000. Preferential dissolution of ^{234}U and radiogenic Pb from α-recoil damaged lattice sites in zircon: implications for thermal histories and Pb isotopic fractionation in the near surface environment. Chemical Geology 162, 41–58.

de Wit, M.J., 1998. On Archaean granites, greenstones, cratons and tectonics: does the evidence demand a verdict? Precambrian Research 91, 181–226.

Dodson, M.H., McClellan-Brown, E., 1985. Isotopic and palaeomagnetic evidence for rates of cooling, uplift and erosion. In: Snelling, N.J. (Ed.), The Chronology of Geological Record: Memoire of the Geological Society of London, 10, pp. 315–325.

Duchesne, J., Wilmart, E., 1997. Igneous charnockites and related rocks from the Bjerkreim–Sokndal layered intrusion (southwest Norway): jotunite (hypersthene–monzodiorite)-derived A-type granitoid suite. Journal of Petrology 38, 337–369.

Dunn, S.J., Nemchin, A.A., Cawood, P.A., Pidgeon, R.T., 2005. Provenance record of the Jack Hills metasedimentary belt. Source of the Earth's oldest zircons. Precambrian Research 138, 235–254.

Ennih, N., Liégeois, J.P., 2008. The boundaries of the West African craton, with special reference to the basement of the Moroccan metacratonic Anti-Atlas belt. Geological Society, London, Special Publications 297, 1–17.

Eriksson, S.C., 1984. Age of the carbonatite and phoscorite magmatism of the Phalaborwa Complex (South Africa). Isotope Geoscience 2, 291–299.

Eriksson, P.G., Banerjee, S., Nelso, D.R., Rigby, M.J., Catuneanu, O., Sarkar, S., Roberts, R.J., Ruban, D., Mtimkulu, M.N., Raju, P.V.S., 2009. A Kaapvaal craton debate: nucleus of an early small supercontinent or affected by an enhanced accretion event? Gondwana Research 15, 354–372.

Feybesse, J.L., Johan, V., Triboulet, C., Guerrot, C., Mayaga-Mikolo, F., Bouchot, V., Eko N'dong, J., 2008. The West Central African belt: a model of 2.5–2.0 Ga accretion and two-phase orogenic evolution. Precambrian Research 87, 161–216.

Foley, S., Tiepolo, M., Vannuci, R., 2002. Growth of early continental crust controlled by melting of amphibolite in subduction zones. Nature 41, 837–840.

Frei, R., Kamber, B.S., 1995. Single mineral Pb–Pb dating. Earth and Planetary Science Letters 129, 261–268.

Frei, R., Villa, I.M., Nägler, T.F., Kramers, J.D., Przybylowizc, W.J., Prozesky, V.M., Hoffmann, B.A., Kamber, B.S., 1997. Single mineral dating by the Pb–Pb step-leaching method: assessing the mechanisms. Geochimica et Cosmochimica Acta 61 (2), 393–414.

Frost, C.D., O'Nions, R.K., 1985. Caledonian magma genesis and crustal recycling. Journal of Petrology 26, 515–544.

Frost, B.R., Barnes, C.G., Collins, W.J., Arculus, R.J., Ellis, D.J., Frost, C.D., 2001. A geochemical classification of granitic rocks. Journal of Petrology 42, 2033–2048.

Geisler, T., Pidgeon, R.T., 2001. Significance of radiation damage on the integral SEM cathodoluminescence intensity of zircon: an experimental annealing study. Neues Jahrbuch für Mineralogie. Monatshefte 10, 33–445.

Goldstein, S.L., O'Nions, R.K., Hamilton, P.J., 1984. A Sm–Nd isotopic study of the atmospheric dust and particulates from major river systems. Earth and Planetary Science Letters 70, 221–236.

Goodwin, A.M., 1991. Precambrian geology — the dynamic evolution of the continental crust. Academic Press. Harcourt Brace Jovanovich Publishers, 666 pp.

Hanchar, J.M., Miller, C.F., 1993. Zircon zoning patterns as revealed by cathodoluminescence and backscattered electron images: implications for interpretation of complex crustal histories. Chemical Geology 110, 1–13.

Hanchar, J.M., Rudnick, R.L., 1995. Revealing hidden structures: the application of cathodoluminescence and backscattered electron imaging to dating zircons from lower crustal xenoliths. Lithos 36, 289–303.

Hansen, B.T., Friderichsen, J.D., 1989. The influence of recent lead loss on the interpretation of disturbed U–Pb systems in zircons from igneous rocks in East Greenland. Lithos 23, 209–223.

Hanski, E.J., Huhma, H., Vuolo, J.I., 2005. SIMS zircon ages and Nd isotope systematics of the 2.22 Ga Mafic intrusions in Northern and Eastern Greenland. In: Vuolo, J., Mertanen, S. (Eds.), 5th International Dyke Conference, 31 July–3 August 2005. Rovaniemi, Finland, p. 20. Abstracts and Programme.

Harrison, T.M., Duncan, I., McDougall, I., 1985. Diffusion of 40Ar in biotite: temperature, pressure and compositional effects. Geochemica et Cosmochemica Acta 49, 2461–2468.

Hegde, V.S., Chavadi, V.C., 2009. Geochemistry of late Archean metagreywackes from the Western Dharwar Craton, South India: implications for provenance and nature of Late Archean crust. Gondwana Research 15, 178–187.

Jacobson, S.B., Wasserburg, G.J., 1980. Sm–Nd isotopic evolution of chondrites. Earth and Planetary Science Letters 50, 139–155.

Kay, S.M., Coira, B., Viramonte, J., 1994. Young mafic back arc volcanic rocks as indicators of continental lithospheric delamination beneath the Argentine Puna plateau, Central Andes. Journal of Geophysical Research 99 (B12), 24323–24339.

Kay, S.M., Abbruzzi, J.M., 1996. Magmatic evidence for Neogene lithospheric evolution of the central Andean "flat-slab" between 30°S and 32°S. Tectonophysics 259, 15–28.

Kampunzu, A.B., Tombale, A.R., Zhai, M., Bagai, Z., Majaule, T., Modisi, M.P., 2003. Major and trace element geochemistry of plutonic rocks from Francistown, NE Botswana: evidence for a Neoarchaean continental active margin in the Zimbabwe craton. Lithos 71, 431–460.

Kempe, U., Gruner, T., Nasdala, L., Wolf, D., 2000. Relevance of cathodoluminescence for the interpretation of U–Pb ages, with an example of an application to a study of zircons from the Saxonian granitoid complex, Germany. In: Pagel, M., Barbin, V., Ohnenstetter, D. (Eds.), Cathodoluminescence in geosciences. Springer, Berlin Heidelberg New York, pp. 415–455.

Klötzli, U.S., 1999. Single zircon evaporation thermal ionisation mass spectrometry: method and procedures. Analyst 122, 1239–1248.

Klötzli-Chowanetz, E., Klötzli, U.S., Koller, F., 1997. Lower Ordovician migmatisation in the Ötztal crystalline basement/Austria: linking U–Pb and Pb–Pb dating with zircon morphology. Schweizerisch Mineralogische–Petrographische Mitteilungen 77, 315–324.

Kober, B., 1986. Whole grain evaporation for $^{207}Pb/^{206}Pb$ age investigations on single zircons using a double-filament thermal ion source. Contributions to Mineralogy and Petrology 93, 482–490.

Kober, B., 1987. Single zircon evaporation combined with Pb^{+} emitter bedding for $^{207}Pb/^{206}Pb$-age investigations using thermal ion mass spectrometry, and implications in zirconology. Contributions to Mineralogy and Petrology 96, 63–71.

Köppel, V., Sommerauer, J., 1974. Trace elements and the behaviour of U–Pb system in inherited and newly formed zircons. Contributions to Mineralogy and Petrology 43, 71–82.

Please cite this article as: Shang, C.K., et al., Late Archaean high-K granite geochronology of the northern metacratonic margin of the Archaean Congo craton, Southern Cameroon: Evidence..., Gondwana Research (2010), doi:10.1016/j.gr.2010.02.008

Kornprobst, J., Lasserre, M., Rollet, M., Soba, D., 1976. Existence au Cameroun d'un magmatisme alcalin Pan-Africain ou plus ancien: la syénite néphélinique de Nkonglong. Comparaison avec les roches alcalines connues dans la même région. Bulletin Société Géologique de France 18 (5), 1295–1305 tome XVIII.

Kramers, J., Frei, R., Newville, M., Kober, B., Villa, I., 2009. On the valency state of radiogenic lead in zircon and its consequences. Chemical Geology 261, 4–11.

Kröner, A., Jaeckel, P., Williams, I.S., 1994. Pb-loss patterns in zircons from a high grade metamorphic terrain as revealed by different dating methods: U–Pb and Pb–Pb ages of igneous and metamorphic zircons from Northern Sri Lanka. Precambrian Research 66, 151–181.

Kröner, A., Jaeckel, P., Brandl, G., Nemchin, A.A., Pidgeon, R.T., 1999. Single zircon ages for granitoid gneisses in the Central Zone of the Limpopo Belt, Southern Africa and geodynamic significance. Precambrian Research 93, 299–337.

Lasserre, M., Soba, D., 1976. Age Libérien des granodiorites et des gneiss à pyroxènes du Cameroun Méridional. Bulletin BRGM 2 (4), 17–32.

Lerouge, C., Cocherie, A., Toteu, S.F., Penaye, J., Milési, J.P., Tchameni, R., Nsifa, E.N., Fanning, M., Deloele, E., 2006. Shrimp U–Pb zircon age evidence for Paleoproterozoic sedimentation and 2.05 Ga syntectonic plutonism in the Nyong Group, South-Western Cameroon: consequences for the Eburnean–Transamazonian belt of NE Brazil and Central Africa. Journal of African Earth Sciences 44, 413–427.

Liégeois, J.P., Navez, J., Hertogen, J., Black, R., 1998. Contrasting origin of post-collisional high-K calc-alkaline and shoshonitic versus alkaline and peralkaline granitoids. Lithos 45, 1–28.

Liégeois, J.P., Latouche, L., Boughrara, M., Navez, J., Guiraud, M., 2003. The LATEA metacraton (Central Hoggar, Tuareg shield, Algeria): behaviour of an old passive margin during the Pan-African orogeny. Journal of African Earth Sciences 37, 161–190.

Liégeois, J.P., Benhallou, A., Azzouni-Sekkal, A., Yahiaoui, R., Bonin, B., 2005. The Hoggar swell and volcanism: reactivation of the Precambrian Tuareg shield during Alpine convergence and West African Cenozoic volcanism. In: Foulger, G.R., Natland, J.H., Presnall, D.C., Anderson, D.L. (Eds.), Plates, Plumes and Paradigms: Geological Society of America Special Paper, 388, pp. 379–400.

Lobach-Zhuchenko, S.B., Chekulaev, V.G., Arestova, N.A., Vrevsky, A.B., Kovalenko, A.V., 2003. Genesis of the earliest (3.20–2.83 Ga) terranes of the Fennoscandian shield. Russian Journal of Earth Science 5, 1–17.

Luais, B., Hawkesworth, C.J., 1994. The generation of continental crust; an intergrated study of crust forming processes in the Archaean of Zimbabwe. Journal of Petrology 35, 43–93.

Ludwig, K., 2003. Isoplot/Ex, version 3.00: a geochronological tool-kit for Microsoft Excel. Berkeley Geochronology Center Special Publications No. 4.

Lugmair, G.W., Marti, K., 1978. Lunar initial $^{143}Nd/^{144}Nd$: differential evolution of the lunar crust and mantle. Earth and Planetary Science Letters 39, 349–357.

Mattinson, J.M., 1994. A study of complex discordance in zircons using step-wise dissolution techniques. Contributions to Mineralogy and Petrology 116, 117–129.

Mattinson, J.M., 2000. Low-temperature U–Pb discordance mechanisms in zircons; the role of radiation damage and fluids. Eos 81 (48, Supplement), 1361–1362.

Maurizot, P., Abessolo, A., Feybesse, J.L., Johan, L.P., 1986. Etude de prospection minière du Sud-Ouest Cameroun. Synthèse des travaux de 1978 à 1985. Rapport de BRGM 85, p. 274.

Mezger, K., 1990. Geochronology in granulites. In: Vielzeif, D., Vidal, Ph. (Eds.), Granulites and crustal evolution 311, pp. 451–470.

Mezger, K., Krogstad, E.J., 1997. Interpretation of discordant U–Pb zircon ages: an evaluation. Journal of Metamorphic Geology 15, 127–140.

Moorbath, S., Kamber, B.S., 1998. A reassessment of the timing of early Archaean crustal evolution in West Greenland. Geology of Greenland Survey Bulletin 180, 88–93.

Möller, A., O'Brien, P.J., Kennedy, A., Kröner, A., 2002. Polyphase zircon in ultrahigh-temperature granulites (Rogaland, SW Norway): constraints for Pb diffusion in zircon. Journal of metamorphic Geology 20, 727–740.

Mpodozis, C., Cornejo, P., Kay, S.M., Titler, A., 1995. La Franja de Maricunga: Sintesis de la evolucion del Frente Volcanico Oligoceno–Mioceno de la zona sur de los Andes Centrales. Revista Geologica Chile 21, 273–313.

Mvondo, H., den Brok, S.W.J., Mvondo Ondoa, J., 2003. Evidence for extension and exhumation of the Yaounde nappe (Pan-African fold belt, Cameroon). Journal of African Earth Sciences 36, 215–231.

Nasdala, L., Lengauer, C.L., Hanchar, J.M., Kronz, A., Wirth, R., Blanc, P., Kennedy, A.K., Seydoux-Guillaume, A.M., 2002. Annealing radiation damage and the recovery of cathodoluminescence. Chemical Geology 191, 121–140.

Nasdala, L., Zhang, M., Kempe, U., Panczer, G., Gaft, M., Andrut, M., Plötze, M., 2003. Spectroscopic methods applied to zircon. In: Hanchar, J.M., Hoskin, P.W.O. (Eds.), zircon: Reviews of Mineralogy and Geochmistry, 53, pp. 427–467.

Nédélec, A., 1990. Late calc-alkaline plutonism in the Archaean Ntem unit: the Sangmelima granodioritic suite (South Cameroon). 15th colloquium on African Geology, Publications Occasionnelle. CIFEG 22, 25–28.

Nédélec, A., Nsifa, E.N., Martin, H., 1990. Major and trace element geochemistry of the Archaean Ntem plutonic complex (South Cameroon): petrogenesis and crustal evolution. Precambrian Research 47, 35–50.

Nelson, B.K., DePaolo, D.J., 1988. Application of Sm–Nd and Rb–Sr isotope systematics to studies of provenance and basin analysis. Journal of Sedimentary Petrology 58, 348–357.

Nemchin, A.A., Whitehouse, M.J., Pidgeon, R.T., Meyer, C., 2006. Oxygen isotopic signature of 4.4–3.9 Ga zircons as a monitor of differentiation processes on the Moon. Geochimica et Cosmochimica Acta 70, 1864–1872.

Ngnotué, T., Nzenti, J.P., Barbey, P., Tchoua, F.M., 2000. The Ntue–Betamba high-grade gneisses: a northward extension of the Pan-African–Yaounde gneisses in Cameroon. Journal of African Earth Sciences 31, 369–381.

Nutman, A.P., Friend, C.R.L., Barker, S.L.L., McGregor, V.R., 2004. Inventory and assessment of Palaeoarchaean gneiss terrains and detrital zircons in southern West Greenland. Precambrian Research 135, 281–314.

Nzenti, J.P., Barbey, P., Macaudière, J., Soba, D., 1988. Origin and evolution of the late Precambrian high-grade Yaounde gneisses (Cameroon). Precambrian Research 38, 91–109.

Ordonez Regil, E., Schleiffer, J.J., Adloff, J.P., Roessler, K., 1989. Chemical effects of α-decay in uranium minerals. Radiochimica Acta 47, 177–185.

Parrish, R.R., 1987. An improved micro-capsule for zircon dissolution in U–Pb geochronology. Chemical Geology 66, 99–102.

Penaye, J., Toteu, S.F., Van Schmus, W.R., Nzenti, J.P., 1993. U–Pb and Sm–Nd preliminary geochronologic data on the Yaounde series, Cameroon: a re-interpretation of the granulitic rocks as a suture of collision in the Central Africa, belt. Compte Rendus de l'Académie des Science de Paris 317, 789–794.

Pidgeon, R.T., 1992. Recrystallization of oscillatory zoned zircon: some geochronological and petrological implications. Contributions to Mineralogy and Petrology 110, 463–472.

Pidgeon, R.T., Nemchin, A.A., 2006. High abundance of early Archaean grains and the age distribution of detrital zircons in a sillimanite-bearing quartzite from Mt Narryer, Western Australia. Precambrian Research 150, 201–220.

Pidgeon, R.T., Nemchin, A.A., van Bronswijk, W., Geisler, T., Meyer, C., Compston, W., Williams, I.S., 2007. Complex history of a zircon aggregate from lunar breccia 73235. Geochimica Cosmochimica Acta 71, 1370–1381.

Pin, C., Poidevin, J.L., 1987. U–Pb zircon evidence for Pan-African granulite facies metamorphism in the Central African Repulblic. A new interpretation of the high grade series of the northen border of the Archaean Congo carton. Precambrian Research 36, 303–312.

Pouclet, A., Tchameni, R., Mezger, K., Vidal, M., Nsifa, E.N., Shang, C.K., Penaye, J., 2007. Archaean crustal accretion at the northern border of the Congo craton (South Cameroon). The charnockite-TTG link. Bulletin of the Geological Society of France 178, 331–342.

Pupin, J.P., 1980. Zircon and granite Petrology. Contributions to Mineralogy and Petrology 73, 207–220.

Rapp, P.R., Watson, E.B., Mille, C.F., 1991. Partial melting of amphobolite/eclogite and the origin of Archaean trondhjemites and tonalites. Precambrian Research 94, 4619–4633.

Ritzwoller, M.H., Shapiro, N.M., Barmin, M.P., Levshin, A.L., 2002, Global surface wave diffraction tomography. Journal of Geophysical Research 107, 2335-ESE-4.1-4.13.

Rubatto, D., 2002. Zircon trace element geochemistry: partitioning with garnet and link between U–Pb ages and metamorphism. Chemical Geology 184, 123–138.

Rubatto, D., Gebauer, D., 2000. Use of cathodoluminescence for U–Pb zircon dating by ion microprobe: some examples from the western Alps. In: Pagel, M., Barbin, V., Ohnenstetter, D. (Eds.), Cathodoluminescence in geosciences. Springer, Berlin Heidelberg New York, pp. 373–400.

Rushmer, T., 1991. Partial melting of two amphibolites: contrasting experimental results under fluid absent conditions. Contributions to Mineralogy and Petrology 107, 41–59.

Shang, C.K., 2001. Geology, geochemistry and geochronology of Archaean rocks from the Sangmelima Region, Ntem complex, NW Congo craton, South Cameroon. Ph.D Thesis, University of Tübingen, Germany, pp. 313.

Shang, C.K., Satir, M., Siebel, W., Taubald, H., Nsifa, E.N., Westphal, M., Reitter, E., 2001. Genesis of K-rich granitoids in the Sangmelima region, Ntem complex (Congo craton), Cameroon. Terra Nostra 5, 60–63.

Shang, C.K., Satir, M., Siebel, W., Nsifa, E.N., Taubald, H., Liegeois, J.P., Tchoua, F.M., 2004a. Major and trace element geochemistry, Rb–Sr and Sm–Nd systematics of TTG magmatism in the Congo craton: case of the Sangmelima region, Ntem complex, southern Cameroon. Journal of African Earth Sciences 40, 61–79.

Shang, C.K., Siebel, W., Satir, M., Chen, F., Mvondo, J.O., 2004b. Zircon Pb–Pb and U–Pb systematics of TTG rocks in the Congo craton: constraints of crustal formation, crystallization and Pan-African lead loss. Bulletin of Geosciences 79, 205–219.

Shang, C.K., Satir, M., Nsifa, E.N., Liegeois, J.P., Siebel, W., Taubald, H., 2007. Archaean high-K granitoids produced by remelting of the earlier Tonalite–Trondhjemite–Granodiorite (TTG) in the Sangmelima region of the Ntem complex of the Congo craton, southern Cameroon. International Journal of Earth Sciences 96, 817–842.

Shapiro, N.M., 2004. Surface wave diffraction tomography map generated from the CUB model. http://ciei.colorado.edu/~nshapiro/MODEL/.

Shapiro, N.M., Ritzwoller, M.H., 2002. Monte-Carlo inversion for a global shear velocity model of the crust and upper mantle. Geophysical Journal International 151, 88–105.

Sharma, R.S., Pandit, M.K., 2003. Evolution of early continental crust. Current Science 84, 995–1001.

Sinha, A.K., Wayne, D.M., Hewitt, D.A., 1992. The hydrothermal stability of zircon: preliminary experimental and isotopic studies. Geochimica et Cosmochimica Acta 56, 3551–3560.

Sláma, J., Košler, J., Condon, D.J., Crowley, J.L., Gerdes, A., Hanchar, J.M., Horstwood, S.A., Morris, G.A., Nasdala, L., Norberg, N., Schaltegger, U., Schoene, B., Tubrett, M.N., Whitehouse, M.J., 2008. Plešovice zircon — a new natural reference material for U–Pb and Hf isotopic analysis. Chemical Geology 249, 1–35.

Stacey, J.S., Kramers, J.D., 1975. Approximation of terrestrial lead isotope evolution by a two-stage model. Earth and Planetary Science Letters 26, 207–221.

Steiger, R.H., Jäger, E., 1977. Subcommision on geochronology: conventions of the use of decay constants in geochronology and cosmochronology. Earth and Planetary Science Letters 36, 359–362.

Stern, T.W., Goldich, S.S., Newell, M.F., 1966. Effect of weathering on the U–Pb ages of zircon from the Morton Gneiss, Minnesota. Earth and Planetary Science Letters 1, 369–371.

Takam, T., Arima, M., Kokonyangi, J., Dunkley, D.J., Nsifa, E.N., 2009. Paleoarchaean charnockites in the Ntem complex, Congo craton, Cameroon: insights from SHRIMP zircon U–Pb ages. Journal of Mineralogical and Petrological Sciences 104, 1–11.

Please cite this article as: Shang, C.K., et al., Late Archaean high-K granite geochronology of the northern metacratonic margin of the Archaean Congo craton, Southern Cameroon: Evidence..., Gondwana Research (2010), doi:10.1016/j.gr.2010.02.008

Tchameni, R., Mezger, K., Nsifa, N.E., Pouclet, A., 2000. Neoarchaean evolution in the Congo craton: evidence from K rich granitoids of the Ntem complex, Southern Cameroon. Journal of African Earth Sciences 30, 133–147.

Tepper, J.H., Nelson, B.K., Bergantz, G.W., Irving, A.J., 1993. Petrology of the Chilliwack batholith, North Cascades, Washington: generation of calc-alkline granitoids by melting of mafic lower crust with variable water fugacity. Contributions to Mineralogy and Petrology 113, 333–351.

Tetsopgang, T., Suzuki, K., Njonfang, E., 2008. Petrology and CHIME geochronology of Pan-African high K and Sr/Y granitoids in the Nkambe area, Cameroon. Gondwana Research 14, 686–699.

Toteu, S.M., Van Schmus, W.R., Penaye, J., Nyobe, J.B., 1994. U–Pb and Sm–Nd evidence for Eburnian and Pan-African high grade metamorphism in cratonic rocks of Southern Cameroon. Precambrian Research 67, 321–347.

Toteu, S.F., Van Schmus, W.R., Penaye, J., Michard, A., 2001. New U–Pb and Sm–Nd data from north-central Cameroon and its bearing on the pre-Pan African history of central Africa. Precambrian Research 108, 45–73.

Toteu, S.F., Yongue, R.F., Penaye, J., Tchakounte, J., Seme Mouangue, A.C., Van Schmus, W.R., Deloule, E., Stendal, H., 2006. U–Pb dating of plutonic rocks involved in the nappe tectonic in southern Cameroon: consequence for the Pan-African orogenic evolution of the central African fold belt. Journal of African Earth Sciences 44, 479–493.

van Breemen, O., Henderson, J.B., Loveridge, W.D., Thompson, P.H., 1987. U–Pb zircon and monazite geochronology and zircon morphology of granulite and granite from the Thelon tectonic zone, Healey Lake map areas, N.W.T. Current Research Part A: Geological Survey of Canada, 87-1A, pp. 783–801.

Vavra, G., 1990. On the kinematics of zircon growth and its petrogenetic significance: a cathodoluminescence study. Contributions to Mineralogy and Petrology 106, 90–99.

Vavra, G., Gebauer, D., Schmid, R., Compston, W., 1996. Multiple zircon growth and recrystallization during polyphase Late Carboniferous to Triassic metamorphism in granulites of the Ivrea Zone (Southern Alps): an ion microprobe (SHRIMP) study. Contributions to Mineralogy and Petrology 122, 337–358.

Verwoerd, W.J., 1986. Mineral deposits associated with carbonatites and alkaline rocks. In: Anhaeusser, C.R., Maske, S. (Eds.), Mineral deposits of Southern Africa, II. Geological Society of South Africa, Johannesburg, pp. 2173–2191.

Vicat, J.P., Leger, J.M., Nsifa, E., Piguet, P., Nzenti, J.P., Tchameni, R., Pouclet, A., 1996. Distinction au sein du craton congolais du Sud-Ouest du Cameroun, de deux épisodes doléritiques initiant les cycles orogéniques éburnéen (Paléoprotérozoïque) et Pan-Africain (Néoprotérozoïque). Compte Rendu de l'Académie des Sciences Paris 323, 575–582 série IIa.

Wickham, S.M., 1987. The generation and emplacement of granitic magmas. Journal of the Geological Society of London 144, 281–297.

Whitehouse, M.J., Kamber, B.S., Moorbath, S., 1999. Age significance of U–Th–Pb zircon data from early Archaean rocks of west Greenland — a reassessment based on combined ion-probe and imaging studies. Chemical Geology 160, 201–224.

Wiedenbeck, M., Alle, P., Corfu, F., Griffin, W.L., Meier, M., Oberli, F., Von Quadt, A., Roddick, J.C., Spiegel, W., 1995. Three natural zircon standards for U–Th–Pb, Lu–Hf, trace element and REE analyses. Geostandard Newsletter 19, 1–23.

Wolf, M.B., Wyllie, P.J., 1994. Dehydration melting of solid amphibolite at 10 kbar: the effect of temperature and time. Contributions to Mineralogy and Petrology 115, 369–383.

Please cite this article as: Shang, C.K., et al., Late Archaean high-K granite geochronology of the northern metacratonic margin of the Archaean Congo craton, Southern Cameroon: Evidence..., Gondwana Research (2010), doi:10.1016/j.gr.2010.02.008